EC:

Associate Editor Decision: Reconsider after major revisions (26 Jan 2018) by Jens Turowski

Comments to the Author:

Dear authors,

I was lucky to be able to solicit the two original reviewers again. While one of the was entirely happy with your edits, the other has some further questions. These mainly relate to details of the methods and accuracy of the modelling. I expect that the amount of revisions needed to bring the manuscript to a publishable state are moderate. I will likely send out the revised paper to the critical reviewer again for screening, but I don't think another round of full reviews will be necessary (depending on your edits and rebuttal, of course).

Thanks for your efforts and I am looking forward to seeing your revised paper.

All the best, Jens Turowski

AC:

Dr. Turowski, we thank your team and reviewers for their continued diligent work reviewing this manuscript. We have addressed all comments to the best of our ability. The majority of the changes were in clarifying remaining issues raised by R1 and R2, which were mostly editorial in nature. R1C2 was the exception, where R1 raises skepticism concerning the accuracy of our model results that consider vegetation drag. Skepticism is certainly warranted. We cite the literature that has shown accounting for vegetation drag in a manner similar to our approach is more accurate and appropriate than traditional roughness approaches, starting p. 3, L14 of the introduction. However, our objective is not to illustrate improved accuracy with the use of the model. Rather, our study applies a framework, tested by others, to a field setting to understand potential interactions between vegetation, flow, and channel-bend flow dynamics (p. 3, L30). Such field studies are sparse. As such, the accuracy of our model will need to be tested in additional studies. Our results provide a framework to do so by making testable predictions about how rivers with bare vs. vegetated bars behave. We believe this work is valuable in spite of its caveats, which we fully acknowledge.

Sincerely,

Sharon, Rebecca, and Andrew

Report #1

The authors have responded clearly to my comments and have improved the manuscript. However, I still have a
few concerns regarding the methods used.

R1C1:

1. Unfortunately I still cannot work out the precise meaning of the text in the supplementary material, describing the gridding process. This may seem like a minor point, and I apologise if I am missing something, but I think it is important as others may wish to reproduce the modelling methods. It appears from the text that a curvilinear grid was created from the topography (2.5m); the authors then ran the model in Cartesian co-ordinates (topography mapped from the previous grid?) and then mapped these Cartesian velocities back on to a different curvilinear grid with higher resolution (2m)? The text suggests Cartesian velocities (Pg 8,Ln 17. Figs 3 &4) but the text also mentions that FASTMECH solves in streamwise and cross-stream co-ordinates (Pg 7, Ln 4-5)? Therefore, could the authors clarify:

• Was the hydraulic model run in Cartesian or orthogonal curvilinear co-ordinates? Why were two grid conversions
required?

• What is meant by the "average cell size" (Supp pg 1, Ln 13) if "the grid size was constant for the whole domain"
(Supp pg 1, Ln 15)? Does it mean constant area but not constant length/width?

• What precisely is meant by "unable to maintain a curvilinear, channel-fitted grid (nodes overlapped)"

AC1:

FASTMECH indeed does solve streamwise and cross-stream coordinates on an orthogonal curvilinear grid. To create the grid, the user picks a centerline, the width of the grid, and then can change the number of i's and j's. Here is a screenshot of what this looks like.

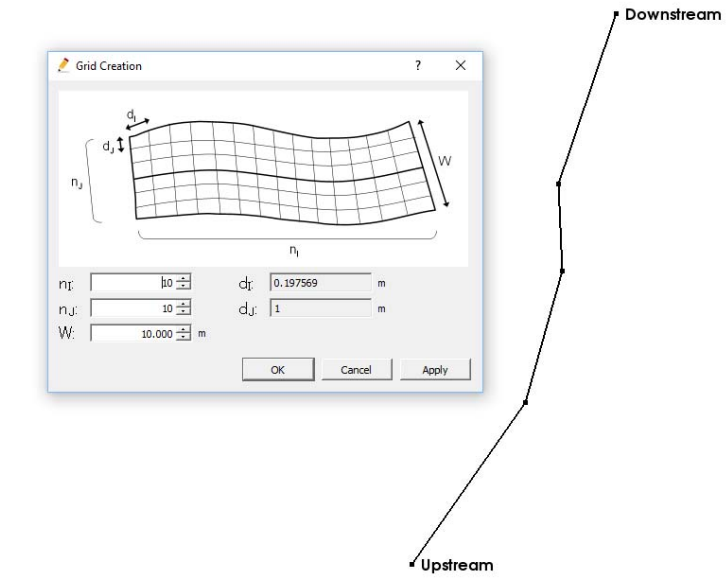

The solver manual (and the developers, personal communication) suggest not picking the exact centerline of the channel, as this is not practical. We provide an example below that is extreme but illustrative:

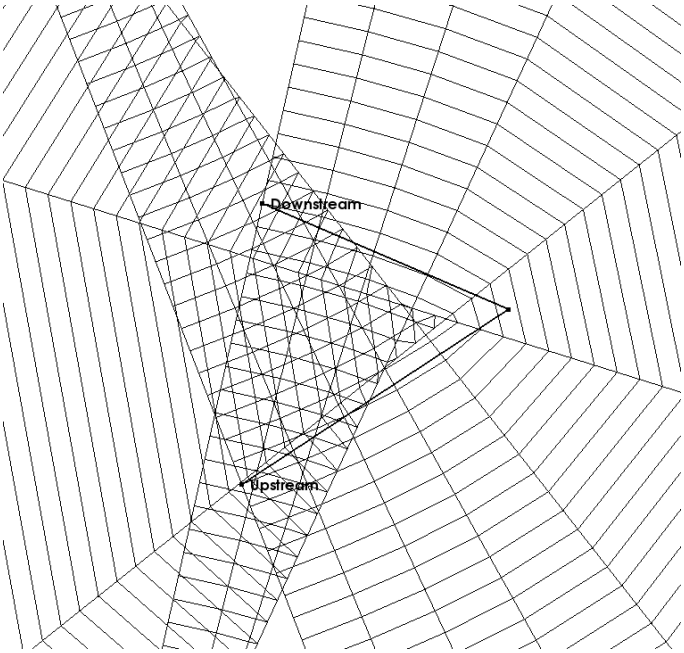

Because a sharp bend is present, the nodes overlap and the grid cannot be created.

Instead of following the exact center of the channel, it is recommended that one picks the "centerline" in more practical terms, such that on average, the grid and model domain is centered over the area of interest. Here is our model domain:

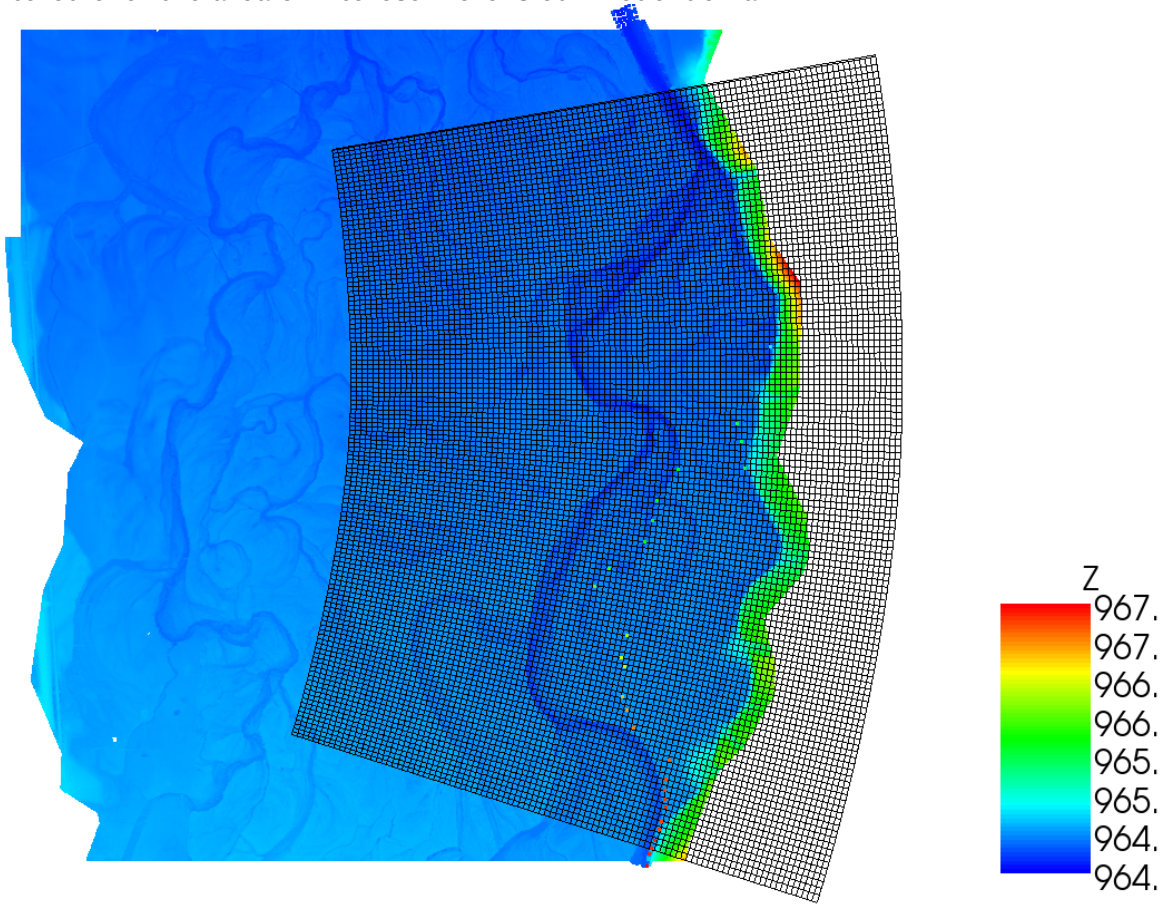

The center of our grid is more or less over the channel, but cannot follow the center of the channel exactly or the nodes will overlap. Thus, the model was run on an orthogonal curvilinear grid, but not one that follows the channel bend of interest. Thus, the results (relative to a Cartesian grid; an output option in FaSTMECH) were rotated to one fitting the channel bend of interest. So only one conversion was done.

The image of our grid shows that the cells are not exactly the same size, thus the "average" value. The terminology "The grid size was constant for the whole domain" is perhaps misleading. We meant that we did not "change resolution" anywhere along the centerline, but this was not clear. We deleted this sentence.

The grid on which the solution output was projected was higher resolution (2 by 2 m) simply so the grid of solutions were not overly averaged by projecting onto a coarse grid.

We have made some revisions to the supplement. If this is still unclear (here or in the manuscript/supplement) please let us know how we might make this clearer.

R1C2:

2. In response to my initial comments, the authors confirm that for the comparison case in the calibration, the unvegetated model outperforms the vegetated model. This is not necessarily surprising if the un-vegetated model has been pre-calibrated using C_d (i.e. vegetation possibly already accounted for in bed C_d). However, it does question the accuracy and usefulness of the vegetation model component and the resulting analysis. I agree that even if the vegetation model shows a higher RMSE in WSE, it might perform better at predicting local velocities, but I cannot see any evidence of this presented here. The results show that the vegetation model produces different results, but not necessarily more accurate results. Is it possible to use the field data to show that the vegetation model enhances prediction of local velocity patterns (i.e. apply the vegetation model at a different discharge where velocity data are available for calibration/validation)? At present, although I follow the logic of model development, based on the evidence presented I find the case for the application of the vegetation model unconvincing

AC2:

We agree that this model imperfectly represents field / flood / vegetation conditions, and that skepticism is appropriate. The velocity calibration data, for example, were only collected during a low-flow condition, not during vegetation inundation, when collection of velocity data would have been challenging from a logistics and safety perspective. We maintain that the results of the study are still useful in making predictions about how a channel with a vegetated bar may behave differently than an unvegetated one, but the model will need more testing. We have defined future research objectives p. 20, L13. Please also see EC response.

R1C3:

3. It would be helpful to include the drag equation in its area-averaged form rather than in the single stem form given, so that the stem density, which is listed as a key variable, appears explicitly, as it would have done in the actual model equation. I expect it would look something like that in Nepf (1999, as already cited in the text) although that paper states it per unit mass.

AC3:

We added stem density to the drag equation in order to represent the true drag force per unit area (i.e., stem area * # of stems in a square meter).

R1C4:

4. In Figure 5 what is the j co-ordinate unit, cells? and is j defined as the cross-stream co-ordinate in the text?
Might units of metres be better for comparing with other figures?

AC4:

The j co-ordinates were defined in one of the iterations… Looks like it accidently got removed! We have changed this to distance in the figures and thus removed the j coordinate notation.

R1C5:

5. Pg 20 Line 11: typo: “…to be most…”
AC5:
Done

Report #2

I have read both versions of the submitted manuscript and think that the authors have addressed all of my previous major concerns. I only have minor editorial comments to help with clarification of some points.

R2C1:
Page 3, lines 14-29: I am a little confused about the topic of this paragraph, it begins with discussing how simply adding vegetation resistance corrections can be problematic and that use of cylinder drag may be better. It is clear that Vargas-Luna used cylinders, and presumably Iwasaki et al. did with drag corrections? What about Marjoribanks et al.? Can you clarify?
AC1:
We have clarified these were modeled as cylinders for all studies.

R2C2:
Page 4, line 20: do you mean drainage area "is"
AC2:
Changed

R2C3:
Page 8, line 8, extra period here.
AC3:
Changed

R2C4:
Page 19, line 1: I still think there is some confusion about negative v meaning a decrease in velocity that is carried over from the previous version of the manuscript. In the Figure 7 v becomes more negative to the right of the patch and you state this in the text but in parenthesis, you state that v was reduced by 180%. I don't think this is
true, if it has become more negative, it must have increased? Or am I misunderstanding something? If this is true, can you please make sure to go through all of the cases in which v becomes more negative and make sure that you do not say that it decreased?
AC4:
Thank you for noticing. We have changed throughout.

R2C5:
Page 19, line 9 "Laboratory studies by Blanckaert (2010), representing sharp meander bends, identified relationships between zones of inward versus outward mass transport, transverse bed profiles, and curvature variations" I feel like this statement is pretty general and doesn't actually describe the relations between all of these parameters, which makes it difficult to understand what the main point is here as it relates to your paper and the surrounding sentences. Maybe you could clarify some?
AC5:
The text has been revised to address this comment and more closely fit with rest of our paper; new text is: "Laboratory studies by Blanckaert (2010), representing sharp meander bends, illustrated that curvature-induced secondary flow associated with topographic steering concentrates most discharge over the deepest, outer parts of a bend and influences bed topography via vertical, downwelling velocities that contribute to pool scour and inward, near-bed velocities that help maintain steep, transverse bed slopes."

R2C6:
Page 20, first paragraph: This seems to be more of a restatement of the results than a discussion of what the results mean, why the results occurred, or how they relate to the previous literature. I am not really clear about the main goal of this paragraph?
AC6:
The main goal of this paragraph was to link our model results to broader work regarding flow steering across meander bends. Upon consideration of both this comment and the previous one (regarding Blanckaert's work), we have reorganized the text so that our

model results regarding flow steering follow directly on the literature discussion (Dietrich and Smith, and Blanckaert) regarding flow steering; this is now the first paragraph of section 4.1.

R2C7:
Page 21, line 7 “Our analysis, more comparable to the flood-dispersed case, shows the potential for development of vegetated islands, but also for prevention of chute cutoff through bar-head maintenance; chute cutoff may be more likely in the absence of vegetation (Constantine et al., 2010).” But your analyses also show that the velocities within a potential chute on the point bar are increased by the presence of vegetation. So the velocity may be lower at the bar head with vegetation, but if velocities are increasing downstream in the incipient chute, couldn’t you have upstream migration of erosion within the chute that counteracts any potential deposition at the bar head? Just a thought….
AC71:
This is an excellent point: as the reviewer recognizes, the literature on chute cutoffs proposes mechanisms whereby cutoffs are initiated at the upstream end of the bar, or by upstream migration within the chute. We have slightly nuanced our text by changing “prevention” to “obstruction,” although we refrain from delving into a deeper discussion of chute cutoff mechanisms here—this is certainly an interesting topic, but one which we consider beyond our scope, and one to which our modeling cannot substantively contribute (although we consider the text here, which was added in response to previous review comments, to be defensible).

R2C8:
Page 21, line 22. Does HIPS abbreviate something? Please define.
AC8:
We have revised the sentence to remove “HIPS” while retaining key content.

R2C9:
Page 21, line 28 Can you please briefly explain this “from increasing bank erosion rates that would tend to increase sinuosity,” Why would higher bank erosion rates result in a higher sinuosity?
AC9:
We agree this sentence was confusing. We have deleted it entirely.

The influence of a vegetated bar on channel-bend flow dynamics

Sharon Bywater-Reyes[1,2], Rebecca M. Diehl[1], Andrew C. Wilcox[1]

[1]Department of Geosciences, University of Montana, 32 Campus Drive #1296, Missoula, Montana, 59812-1296, USA
[2]Department of Earth and Atmospheric Sciences, University of Northern Colorado, 501 20th St., Greeley, Colorado, 80639, USA

Correspondence to: Sharon Bywater-Reyes (sharon.bywaterreyes@unco.edu)

The authors declare that they have no conflict of interest.

Abstract. Point bars influence hydraulics, morphodynamics, and channel geometry in alluvial rivers. Woody riparian vegetation often establishes on point bars and may cause changes in channel-bend hydraulics as a function of vegetation density, morphology, and flow conditions. We used a two-dimensional hydraulic model that accounts for vegetation drag to predict how channel-bend hydraulics are affected by vegetation recruitment on a point bar in a gravel-bed river (Bitterroot River, Montana, United States). The calibrated model shows steep changes in flow hydraulics for vegetated flows compared to bare-bar conditions for flows greater than bankfull up to a 10-year flow (Q_{10}), with limited additional changes thereafter. Vegetation-morphology effects on hydraulics were more pronounced for sparse vegetation compared to dense vegetation. The main effects were 1) reduced flow velocities upstream of the bar; 2) flow steered away from the vegetation patch with up to a 30 % increase in thalweg velocity; and 3) a shift of the high-velocity core of flow toward the cutbank, creating a large cross-stream gradient in streamwise velocity. These modeled results are consistent with a feedback in channels whereby vegetation on point bars steers flow towards the opposite bank, potentially increasing bank erosion at the mid- and downstream end of the bend while simultaneously increasing rates of bar accretion.

1 Introduction

Channel-bend morphodynamics along meandering rivers influence channel morphology, river migration rates, channel-floodplain connectivity, and aquatic habitat. River point bars, fundamental to channel-bend morphology (Blondeaux and Seminara, 1985; Ikeda et al., 1981), steer flow and induce convective accelerations (Dietrich and Smith, 1983) that influence boundary shear stress (Dietrich and Whiting, 1989) and sediment transport fields (Dietrich and Smith, 1983; Legleiter et al., 2011; Nelson and Smith, 1989). Channel migration rates are furthermore controlled by the collective processes of bar accretion and bank erosion. Bars along the inner bends of river meanders, although typically broadly described as point bars, also comprise chute bars, tail bars, ~~chute bars,~~ and scroll bars that reflect distinct formative conditions (e.g., obstructions and/or stream power variations) and produce distinct morphodynamic feedbacks (Kleinhans and van den Berg, 2011).

Channel dynamics can be tightly coupled with the recruitment and succession of riparian vegetation on river bars (Amlin and Rood, 2002; Eke et al., 2014; Karrenberg et al., 2002; Nicholas et al., 2013; Rood et al., 1998). Plants change local hydraulics (Nepf, 2012; Rominger et al., 2010) and sediment transport conditions (Curran and Hession, 2013; Manners et al., 2015; Yager and Schmeeckle, 2013), resulting in strong feedbacks between the recruitment and growth of woody riparian vegetation and bar building (Bendix and Hupp, 2000; Dean and Schmidt, 2011) that can influence the morphology of rivers at multiple scales (Bywater-Reyes et al., 2017; Osterkamp et al., 2012). Pioneer vegetation can occur on all bar types but is most likely to survive on nonmigrating bars, such as forced alternating point bars (Wintenberger et al., 2015). Plant traits including height, frontal area, and stem flexibility vary with elevation above the baseflow channel, influencing both the susceptibility of plants to uprooting during floods and their impact on morphodynamics (Bywater-Reyes et al., 2015, 2017; Diehl et al., 2017a; Kui et al., 2014). Vegetation effects on hydraulics, bank erosion, and channel pattern also depend on the uniformity of vegetation distribution on bars, which can vary depending on wind versus water-based dispersal mechanisms (Van Dijk et al., 2013), and on whether plants occur individually or in patches (Manners et al., 2015).

Experimental work in flumes has shown that vegetation is vital to sustaining meandering in coarse-bedded rivers (Braudrick et al., 2009). Vegetation's effect on stabilizing banks, steering flow, and impacting morphodynamics furthermore depends on seed density and stand age. Uniform vegetation on bars has been shown, experimentally, to decrease bank erosion rates, stabilize banks, and increase sinuosity of meander bends (Van Dijk et al., 2013). Gran and Paola (2001) showed that vegetation, by increasing bank strength, generates secondary currents associated with oblique bank impingement that may be more important than helical flows generated by channel curvature. Other experiments have generally suggested vegetated bars decrease velocities over the bar and push flow toward the outer bank. For example, tests in a constructed, meandering laboratory stream with two reed species planted on a sandy point bar showed that vegetation reduced velocities over the vegetated bar, increased them in the thalweg, strengthened secondary circulation, and directed secondary flow toward the outer bank (Rominger et al., 2010). Another study in the same experimental facility, but using woody seedlings planted on the point bar, also found reduced velocities in the vegetated area of the bar, with the greatest reductions at the upstream end, and the effect varying with vegetation architecture and density (Lightbody et al., 2012). In a flume study where meandering effects were simulated in a straight channel by placing dowels representing vegetation patches in alternating locations along the edges of the flume, vegetation reduced velocity within and at the edges of the vegetation patch and increased velocities near the opposite bank (Bennett et al., 2002). Experiments in a high-curvature meandering flume, in contrast, showed that vegetation inhibited high shear-stress values from reaching the outer bank (Termini, 2016), inconsistent with studies simulating moderate sinuosity channels.

Vegetation's effect on river morphodynamics has~~ve~~ also been simulated with computational models. Reduced-complexity models that approximate the physics of flow have successfully reproduced many of the features observed in channels influenced by vegetation, such as the development of a single-thread channel (e.g., Murray and Paola, 2003). Two-dimensional models that use shallow-water equations and, in some cases, sediment transport relations, provide an alternative that may be less dependent on initial conditions and more capable of representing the physics of vegetation-flow interactions

(Boothroyd et al., 2016, 2017; Marjoribanks et al., 2017; Nelson et al., 2016; Nicholas et al., 2013; Pasternack, 2011; Tonina and Jorde, 2013). Investigations of channel-bend dynamics influenced by vegetation using two-dimensional models often represent vegetation by increasing bed roughness (see Green, 2005 and Camporeale et al., 2013 for comprehensive reviews). Nicholas et al. (2013) simulated bar and island evolution in large anabranching rivers using a morphodynamic model of sediment transport, bank erosion, and floodplain development on a multi-century timescale, where vegetation was modeled using a Chezy roughness coefficient. Asahi et al. (2013) and Eke et al. (2014) modeled river bend erosional and depositional processes that included a bank-stability model and deposition dictated by an assumed vegetation encroachment rule. Bertoldi and Siviglia (2014) used a morphodynamic model coupled with a vegetation biomass model, which accounted for species variations in nutrient and water needs to simulate the coevolution of vegetation and bars in gravel-bed rivers. Vegetation was modeled as increased bed roughness via the Strickler-Manning relation that varied linearly with biomass. Their model showed two scenarios: one where flooding completely removed vegetation, and one where vegetation survived floods, resulting in vegetated bars. These two alternative stable states (bare versus vegetated bars) have been found experimentally as well (Wang et al., 2016).

Although the aforementioned models produce many of the features of river morphodynamic evolution, when vegetation drag is dominant over bed friction, using conventional resistance equations (e.g., Manning's ~~n; roughness~~) to model vegetation's effect on the flow introduces error. Increasing the roughness within vegetated zones increases the modeled shear stress and therefore artificially inflates the sediment transport capacity at the local scale (e.g., vegetation patch or bar), although reach-scale results may be appropriate (Baptist et al., 2005; James et al., 2004). Vegetation drag can also be treated in computational models by representing plants explicitly as cylinders (e.g., Baptist et al., 2007; Vargas-Luna et al., 2015a), comparable to the approach of many flume studies, or by accounting for drag from foliage, stems, and streamlined vegetation, but such an approach is currently not widely adopted because of limited ability to specify all parameters (e.g., Boothroyd et al., 2015, 2017; Jalonen et al., 2013; Västilä and Järvelä, 2014). Vargas-Luna et al. (2015a) showed, through coupling of numerical modeling and experimental work, that representing vegetation as cylinders is most appropriate for dense vegetation. Iwasaki et al. (2015) used a two-dimensional model that accounted for vegetation drag (as cylinders) to explain morphological change of the Otofuke River, Japan, caused by a large flood event in 2011 that produced substantial channel widening and vegetation-influenced bar building. They found that vegetation allowed bar-induced meandering to maintain moderate sinuosity, whereas in the absence of vegetation, river planform would switch from single-thread to braided. Marjoribanks et al. (2017) modeled the effects of vegetation mass blockage and drag, specifying vegetation as cylinders, ~~on channel hydraulics~~ for a small (~5 m wide by 16 m long), straight river reach, and found velocity reduced broadly throughout the channel.

As the above review suggests, there have been considerable advances in laboratory and computational modeling of vegetation effects on hydraulics that complement understanding of bar and bend morphodynamics and reciprocal interactions between riparian vegetation and river processes (Corenblit et al., 2007; Gurnell, 2014; Osterkamp and Hupp, 2010; Schnauder and Moggridge, 2009). Challenges persist, however, in representing field-scale complexities in a modeling framework that

allows for testing field-scale interactions between plants, flow, and channel morphology on vegetated point bars. Here we tackle key elements of this problem by investigating how the distribution of woody vegetation on a point bar influences bend hydraulics and flow steering across a range of flood magnitudes using a two-dimensional modeling approach informed by high-resolution topography and vegetation morphology data that spatially defines vegetation drag. We model a range of vegetation densities and plant morphologies representing different stages of pioneer woody vegetation growth on a point bar. We vary discharge in the model to represent the stage-dependent effects of vegetation on hydraulics, as well as different flood stages that may be important for the recruitment of plants and the erosion or deposition of sediment within the channel bend. We predict that the presence of woody vegetation affects bar and meander dynamics by steering flow, thereby influencing the morphodynamic evolution of vegetated channels. Our objectives are to 1) Determine which vegetation morphology and flow conditions result in the greatest changes to channel-bend hydraulics; and 2) Infer how these changes in hydraulics would impact channel-bend morphodynamics and evolution. The insights derived from our analysis are relevant for understanding ecogeomorphic feedbacks in meandering rivers, understanding how such feedbacks are mediated by plant traits and flow conditions, and for riparian plant species management along river corridors.

2 Methods

2.1 Study area

To meet our objectives, we model a point bar-bend sequence on the Bitterroot River, southwest Montana, United States (Fig. 1). Our field site has a pool-riffle morphology and a wandering pattern, with channel bends, point bars, and woody vegetation on bars and floodplains. The study reach is located on a private reserve (MPG Ranch) with minimal disturbance to the channel and floodplain, and flow and sediment supply are relatively unaltered by flow regulation, because the only significant dam in the contributing watershed is ~120 km upstream of the study reach, on a tributary. Annual mean discharge is 68 $m^3 s^{-1}$, bankfull Shields number is 0.03, and median grain size is 23 mm, and drainage area is~~of~~ ~6,200 km^2. Woody bar vegetation is composed of sand bar willow (*Salix* exigua), and cottonwood (*Populus* trichocarpa) seedlings, saplings, and young trees (Fig. 2a, 2c). Ponderosa pine (*Pinus* ponderosa), gray alder (*Alnus* incana), and black cottonwood (*Populus* trichocarpa) comprise mature floodplain forest species.

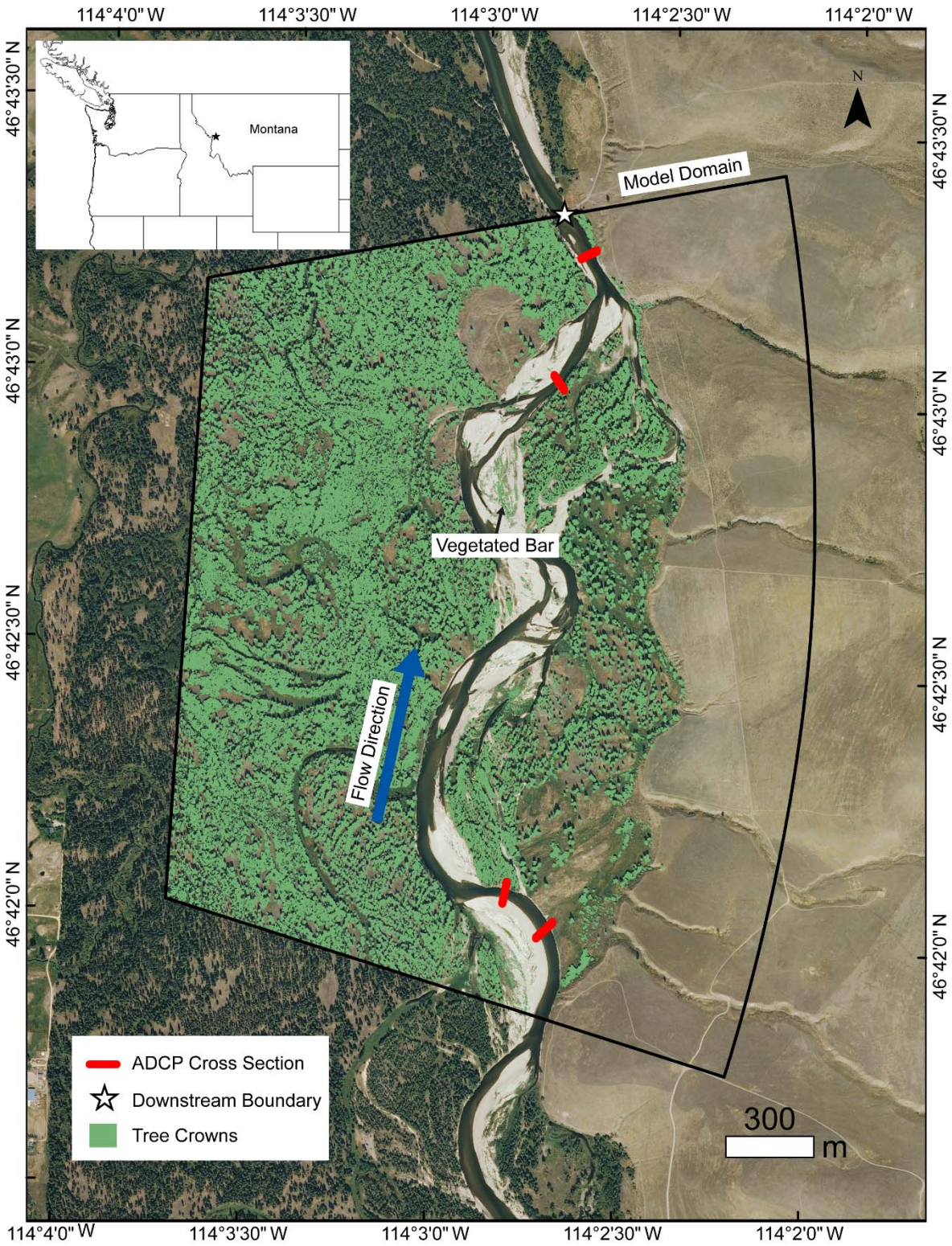
114°4'0" W
114°3'30" W
114°3'0" W
114°2'30" W
114°2'0" W
46°43'30" N
46°43'0" N
46°42'30" N
46°42'0" N
Montana
N
Model Domain
Vegetated Bar
Flow Direction
ADCP Cross Section
Downstream Boundary
Tree Crowns
300
m

Figure 1. Bitterroot River, Montana showing model domain, location of ADCP velocity measurement cross sections, downstream boundary, tree crowns mapped from airborne LiDAR, and the location of the vegetated bar. Inset map shows location in northwestern USA.

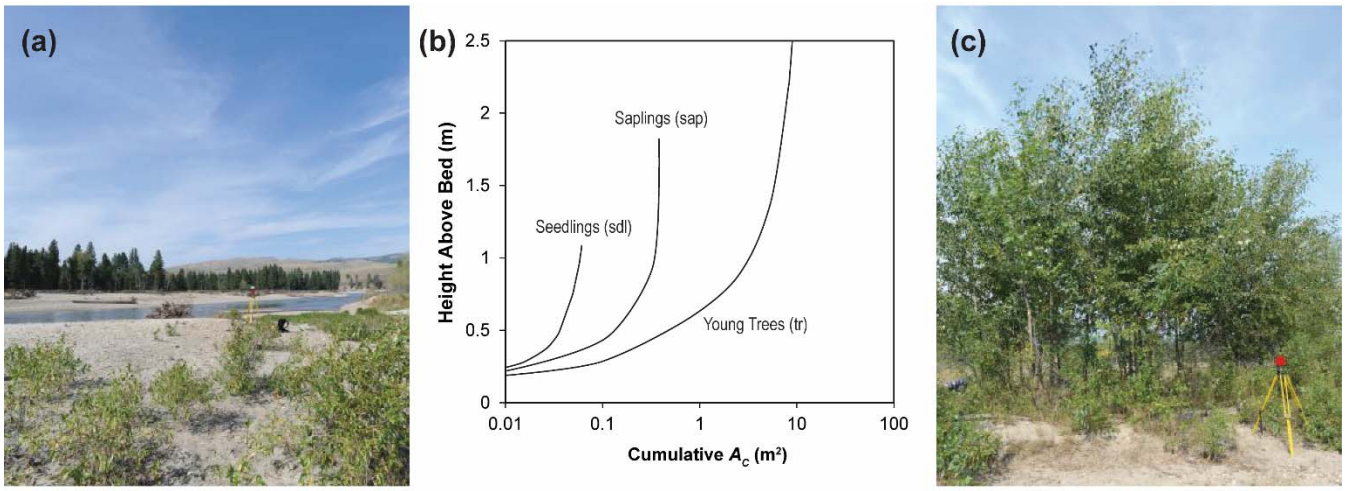

Figure 2. Modeled vegetated bar (a) on the Bitterroot River, showing sparse *Populus* seedlings and saplings. Average cumulative A_c (projected vertical frontal area) of *Populus* varies with height above the bed, and the age and size of the individual (b); the greatest cumulative A_c is reached for young trees (c). The average A_c profile for seedlings (sdl), saplings (sap), and young trees (tr) was used to assign an A_c value based on flow depth for each run. Photo credit: Sarah Doelger.

2.2 Flow model

To characterize the influence of a vegetated bar on channel-bend hydraulics, we used an edited version of FaSTMECH (version 2.3.2), a hydrostatic, quasi-steady flow model contained within iRIC (Nelson et al., 2016; http://i-ric.org/en/index.html). FaSTMECH solves the depth- and Reynolds-averaged momentum equations in the streamwise and cross-stream directions, in a channel-fitted curvilinear coordinate system, using a finite-difference solution (Nelson et al., 2003, 2016). By convention, values of u and v are positive downstream and toward the left bank, respectively. Bed stress closure is achieved through a drag coefficient (C_d) scheme. Details of the modeling process, beyond those provided in the text here, can be found in the Supplement.

We created the flow model domain in FaSTMECH by characterizing the topography and flow boundary conditions (discharge and water surface elevation at the downstream boundary) of a study reach on the Bitterroot River, Montana (Fig. 1). We surveyed channel topography with a combination of airborne LiDAR, echosounder and RTK GPS surveys (see Supplement). The resulting curvilinear orthogonal grid we created had an average cell size of 2.5 by 2.5 m for calibration runs (described below), and 5 by 5 m for the remaining runs. We linked transducer stage measurements at the downstream end of the study reach to discharge derived from USGS gaging station 12344000, Bitterroot River near Darby MT, corrected by contributing area for our field site. Water surface elevations at the downstream boundary for modeled discharges were extracted from the stage-discharge relationship. Discharge was measured at the field site and compared to the adjusted USGS 12344000 value and found to agree within 10 % (Table 1).

Table 1. Calibration flows, showing the channel drag (C_d) and lateral eddy viscosity (LEV), and the root mean square error (RMSE), water surface elevation (WSE), and depth-averaged velocity ($\bar{U}$).

Run	Discharge[a] (m^3 s^{-1})	C_d	LEV	RMSE-WSE[b] (m)
1	48	0.003	0.04	0.11
2	62[c,d]	0.003	0.04	0.11
3	90	0.003	0.04	0.17
4	453[e]	0.003	0.04	0.16
5	453[e,f]	0.003	0.04	0.18

[a]Corrected by contributing area from USGS 12344000
[b]More details on WSE in Supplement
[c]Law-of-the-wall derived $\bar{U}$ had RMSE 0.24 m s^{-1}; mean measured $\bar{U}$ 1.21 m s^{-1}; mean modeled $\bar{U}$ 1.05 m s^{-1} (15 % error); see Supplement for more details
[d]Discharge measured at site was within 10 % of contributing-area-corrected discharge
[e]Q_2 flow
[f]Vegetation model turned on

FaSTMECH uses relaxation coefficients to control changes in a parameter between iterations (Nelson, 2013). Relaxation coefficients were set to 0.5, 0.3, and 0.1 for ERelax, URelax, and ARelax, respectively, through trial and error. Convergence was found after 5000 iterations (mean error discharge < 2 %), considered indicative of adequate model performance for FaSTMECH (Nelson, 2013). We calibrated channel characteristics (bed roughness specified as C_d and lateral eddy viscosity, *LEV*) and considered them fixed after calibration (Table 1). We used a constant C_d, an approach that has been shown elsewhere to perform comparably to variable roughness in FaSTMECH (e.g., Segura and Pitlick, 2015). We set C_d to minimize the root mean square error (RMSE) of modeled water surface elevation (WSE) versus WSE measured in the field from 2011–2015, over a range of calibration flows (see Supplement). In this calibration process we manually varied C_d values from 0.01 to 0.001, resulting in a C_d of 0.003 and lowest RMSE's for WSE from 0.11 to 0.16 m for the lowest and highest calibration flows, respectively (Table 1). Similarly, we manually varied *LEV* from 0.01 to 0.001 during model calibration, resulting in a *LEV* value of 0.04, which minimized RMSE of depth-averaged velocity ($\bar{U}$=0.24 m s^{-1}; Table 1) between modeled values and those measured at four cross sections (Fig. 1) (see Supplement for details). The RMSE ranges obtained through calibration are consistent with values reported in other studies that have used FaSTMECH (e.g., Legleiter et al., 2011; Mueller and Pitlick, 2014; Segura and Pitlick, 2015), providing confidence in model performance.

To address the stage-dependent nature of the impact of a vegetated bar in altering bend hydraulics, we modeled flows with magnitudes corresponding to flows with return periods of 2 (Q_2; 453 m^3 s^{-1}), 10 (Q_{10}; 650 m^3 s^{-1}), 20 (Q_{20}; 715 m^3 s^{-1}) and 100 (Q_{100}; 800 m^3 s^{-1}) years. We converted Cartesian coordinate velocity (U_x, U_y) to streamwise and stream-normal values (Fig. 3; Supplement).

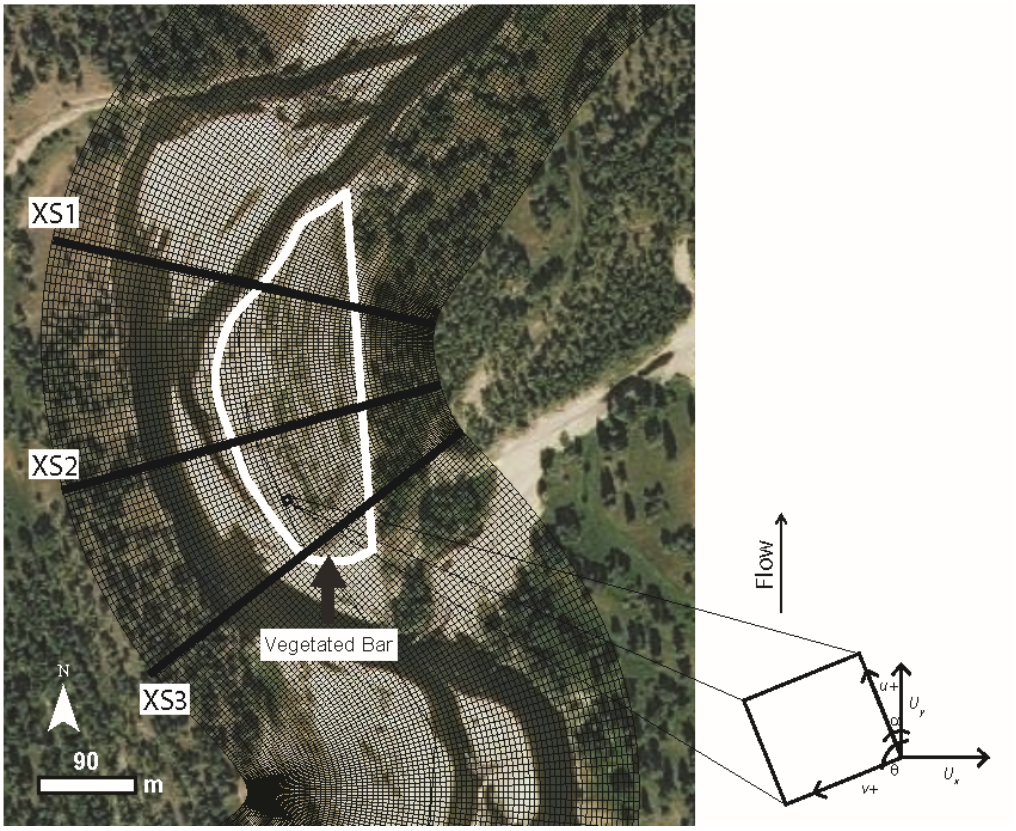

Figure 3. Region around the vegetated bar, showing cross section (XS) locations and the conventions of the curvilinear grid to which model output was converted.

2.3 Modeling vegetation's impact on channel-bend hydraulics

We edited FaSTMECH to account for vegetation form drag (F_D) using the following drag equation for rigid vegetation:

$$F_D = \frac{1}{2}\rho C_{d,v} A_c n U_c^2 \qquad (1)$$

where $C_{d,v}$ is vegetation drag coefficient, A_c is projected vertical frontal area of vegetation (Nepf, 1999; Vargas-Luna et al., 2015, 2016), n is the stem density (#stems m^{-2}), and U_c is the approach velocity. Drag (F_D) is calculated per bed area (distributed over vegetation polygons).

For U_c we used node velocity (after Jalonen et al., 2013). The vegetation drag coefficient ($C_{d,v}$) was assigned a value of one, a first-order approximation also used by others (Boothroyd et al., 2016; Nepf et al., 2013; Vargas-Luna et al., 2016). We modeled vegetation as cylinders by assuming the cylindrical stem frontal area is equal to A_c, specifying vegetation parameters by polygon with an associated ~~stem density (#stems m^{-2})~~ n and height (m; allows for partitioning of A_c by flow depth). The

model assumes a logarithmic velocity profile, although we recognize this is an over-simplification of how factors such as vegetation submergence alter velocity profiles (e.g., Manners et al., 2015).

We focused our analyses on a point bar (Fig. 1) that supports woody riparian vegetation (*Populus* seedlings, saplings, and young trees) most likely recruited mainly by flood dispersal. In our model simulations, we varied vegetation density (#stems m^{-2}) and A_c (m^2 per plant) on the vegetated bar for each of the four flows, and we compared model output to a no-vegetation (no veg) scenario. We considered two vegetation density cases: sparse (*sps*) and dense (*dns*). Our sparse case was based on the average density (0.02 stems m^{-2}) obtained from the airborne LiDAR (see Supplement for more detail). Our dense case (20 stems m^{-2}) was based on the average from random vegetation density plots measured on the bar, which ranged from <1 stem m^{-2} to 227 stems m^{-2} and is consistent with other dense field-measured values (Boyd et al., 2015; van Oorschot et al., 2016; Wilcox and Shafroth, 2013). For A_c, we used ground-based LiDAR to capture vegetation structure (Antonarakis et al., 2010; Bywater-Reyes et al., 2017; Manners et al., 2013; Straatsma et al., 2008). We scanned *Populus* patches representing different stages of pioneer woody vegetation growth: seedlings (*sdl*), saplings (*sap*), and young trees (*tr*). From these scans (postprocessed in the same manner described in (Bywater-Reyes et al., 2017)), we established an A_c – height relationship (Fig. 2b), from which depth-dependent A_c was extracted for each model run by assigning A_c based on the average bar flow depth from the corresponding no-vegetation scenario.

To test whether overbank (floodplain) vegetation (i.e., beyond the vegetated bar) contributes to flow steering in the main channel and influences the hydraulics of the cutbank–bar region of interest (Fig. 3), we included runs with and without floodplain vegetation for each of the four flows and seven bar vegetation scenarios, resulting in 56 model runs. We represented floodplain vegetation as was observed from airborne LiDAR (see Supplement for detail). These analyses showed that the hydraulics of the cutbank–bar region of interest (Fig. 3) were insensitive to whether or not floodplain vegetation (i.e., beyond the vegetated bar) was present across the range of modeled flow conditions. Therefore the descriptions of hydraulics we present in Results are based only on scenarios varying bar vegetation conditions.

We considered hydraulic (u, v) solutions for three cross sections at locations across the bar and cutbank of the channel bend, representing the upstream, midstream, and downstream portion of the bar (Fig. 3). We additionally considered the hydraulics and potential for bed mobility spatially, ~~where the~~using Shields number, τ^*, ~~was used~~ as an indicator of bed mobility:

$$\tau^* = \frac{\tau}{(\rho_s - \rho)gD} \qquad (2)$$

where τ is boundary shear stress, ρ_s is sediment density, g is acceleration due to gravity and $D$is grain diameter. We used the median grain diameter from pebble counts collected on the study bar and along cross sections (Fig. 1). We compared the solutions for vegetation runs for each flow to no-vegetation scenarios to evaluate which configurations had the greatest influence on hydraulics.

3 Results

The effects of point bar vegetation on modeled hydraulics across our study reach are presented here in several ways. First we compare vegetation results, for different density and growth stages, to the no-vegetation case; and second, we compare results spatially at different cross sections across the bar at different discharges. For the no-vegetation case, velocity and shear stress were generally highest in the thalweg and lower over the bar (Fig. 4). Downstream velocity (u) was generally greater than cross-stream velocity (v). The greatest v magnitudes were for the downstream cross section (XS1; Fig. 5c,d). With increasing flow magnitude, both u (Fig. 5b) and v (Fig. 5d) decreased within the thalweg region, but stayed relatively constant over the bar. A similar trend was seen at the mid-bar cross section (XS2) with u decreasing within the thalweg region as flow magnitude increased, but remaining relatively constant over the bar (Fig. 6). In contrast, u increased within the thalweg region and over the bar with increasing flow (Fig. 7a,b) at the upstream cross section (XS3), whereas v stayed relatively constant (Fig. 7c,d).

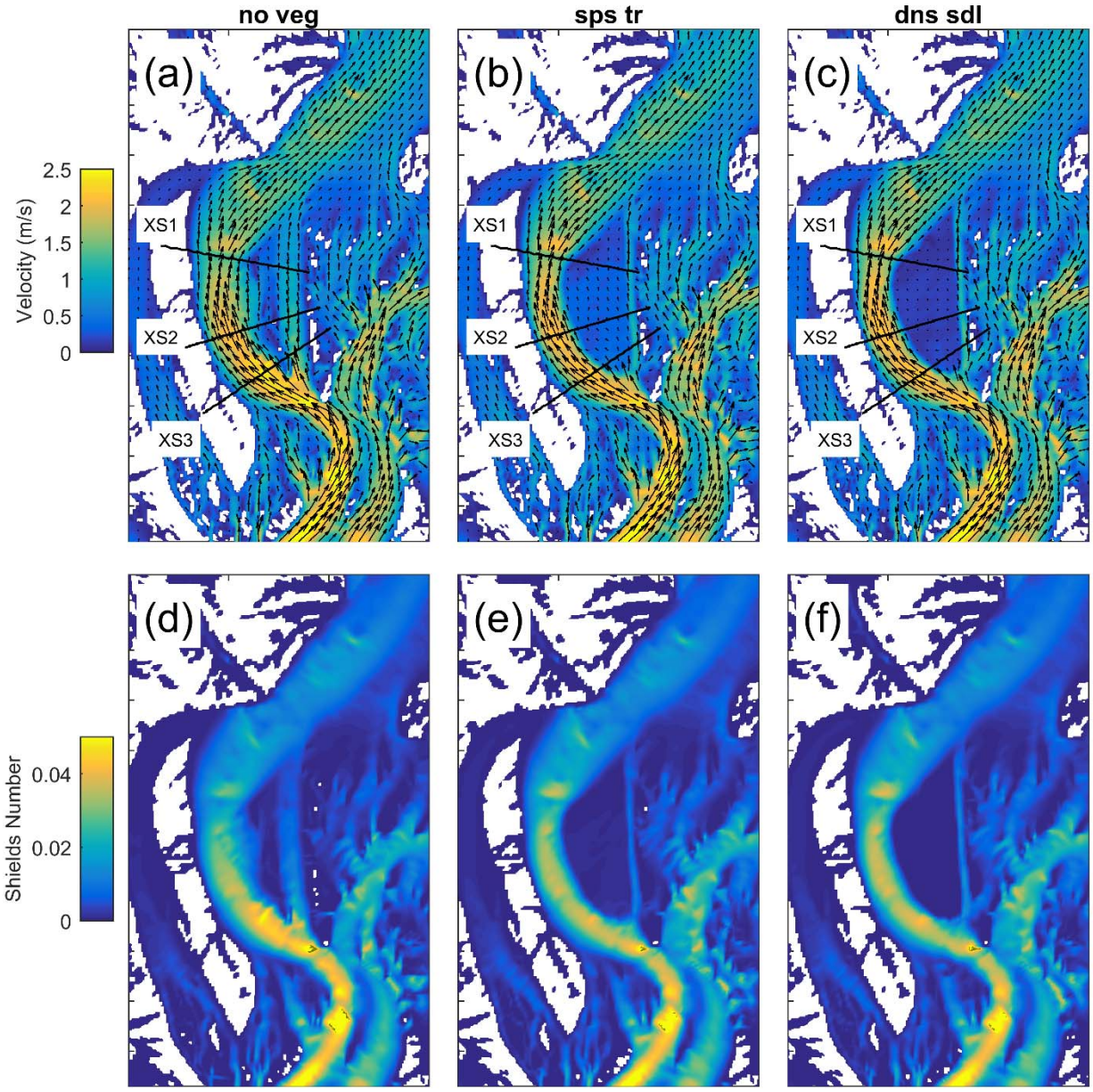

Figure 4. Planview comparison of channel-bend hydraulics (velocity; a–c, and Shields number; d~~e~~–f) for the Q_{10} no-vegetation (a,d), sparse young trees b,e), and dense seedlings (c,f) runs. ~~Location of cross sections (Fig. 3 shown).~~ Velocity and Shields number are reduced on the bar with increasing size or density of plants, and flow paths within the thalweg and adjacent to the vegetation patch become more concentrated.

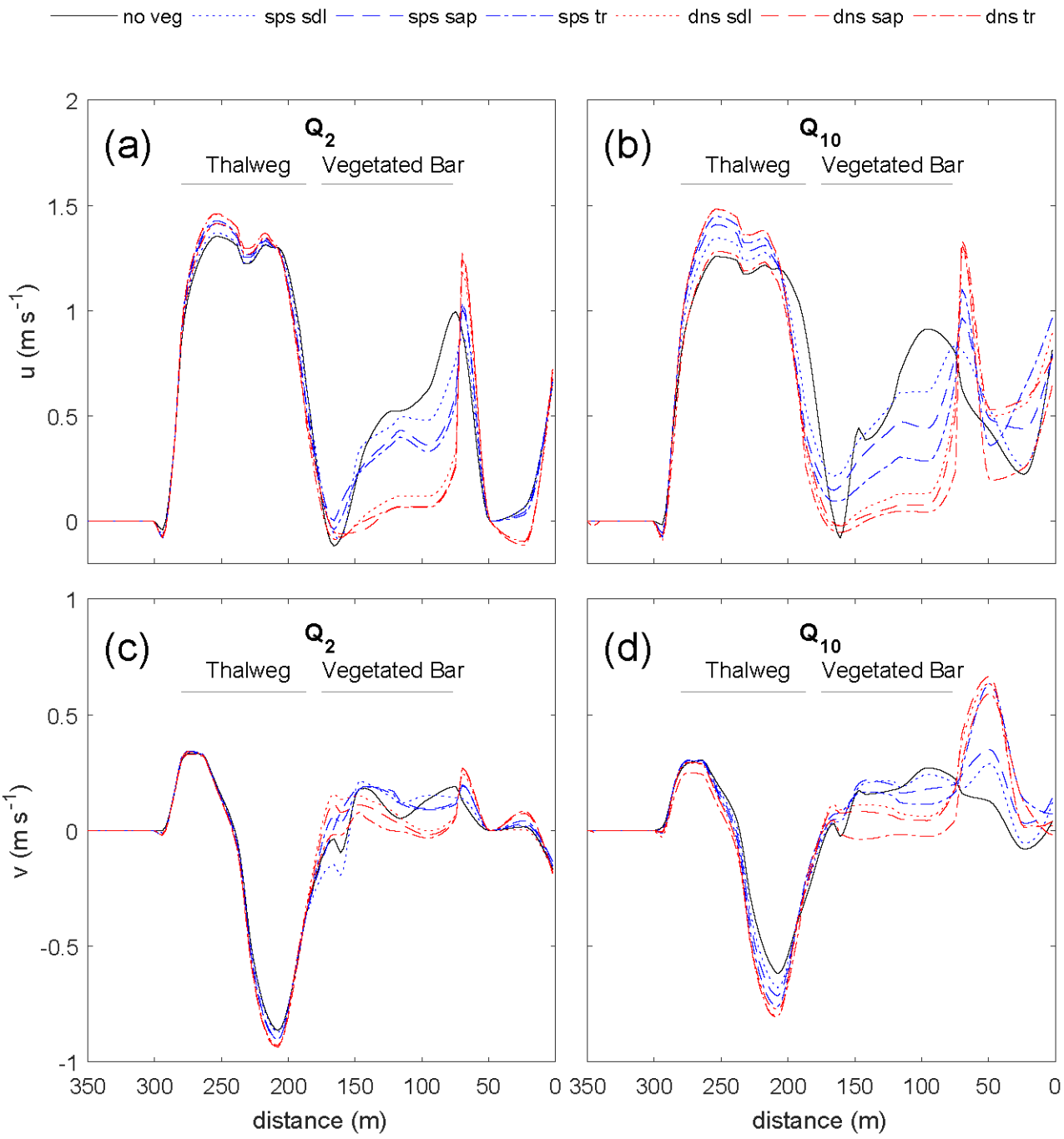
no veg
sps sdl
sps sap
sps tr
dns sdl
dns sap
dns tr
(a)
Q_2
Thalweg
Vegetated Bar
(b)
Q_{10}
Thalweg
Vegetated Bar
(c)
Q_2
Thalweg
Vegetated Bar
(d)
Q_{10}
Thalweg
Vegetated Bar
u (m s^{-1})
v (m s^{-1})
distance (m)
distance (m)

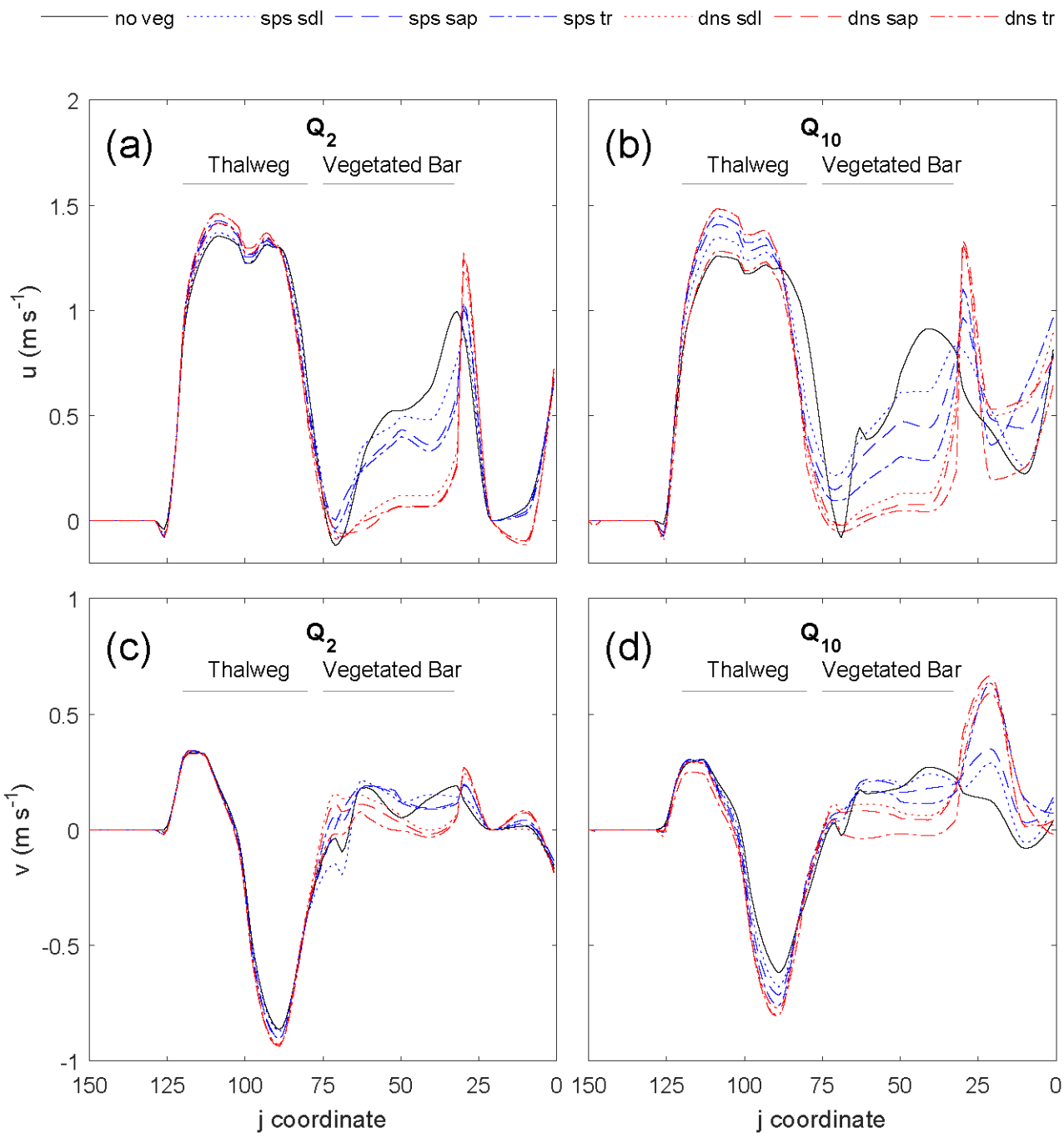

Figure 5. Effect of the vegetated bar ~~(j = 33–75)~~ on the streamwise (*u*; a,b) and stream-normal (*v*; c,d) velocity at the downstream cross section (XS1) for the Q_2 (a,c) and Q_{10} (b,d) flows, with distance from river right end point (Figure 4). With increasing discharge,

plant size (seedling to young trees) and density, *u* is increased and *v* decreased within the thalweg ~~(j = 100)~~. Both *u* and *v* (positive downstream and toward left bank, respectively) are decreased over the bar, and for the sparse young trees and all dense scenarios increased at the edge of the patch.

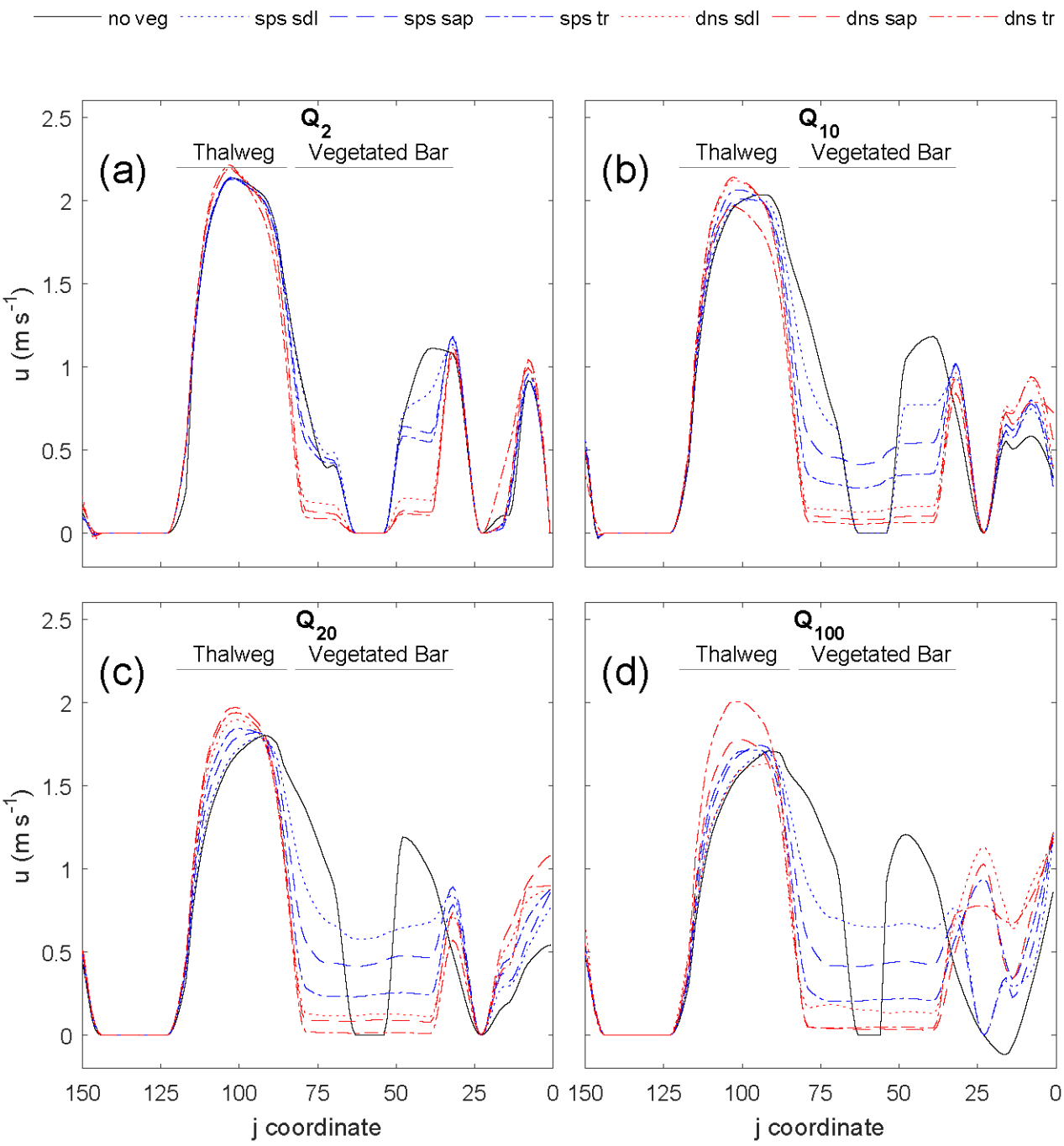
no veg
sps sdl
sps sap
sps tr
dns sdl
dns sap
dns tr
(a)
Q_2
Thalweg
Vegetated Bar
(b)
Q_{10}
Thalweg
Vegetated Bar
(c)
Q_{20}
Thalweg
Vegetated Bar
(d)
Q_{100}
Thalweg
Vegetated Bar
u (m s^{-1})
u (m s^{-1})
0
0.5
1
1.5
2
2.5
150
125
100
75
50
25
0
j coordinate
j coordinate

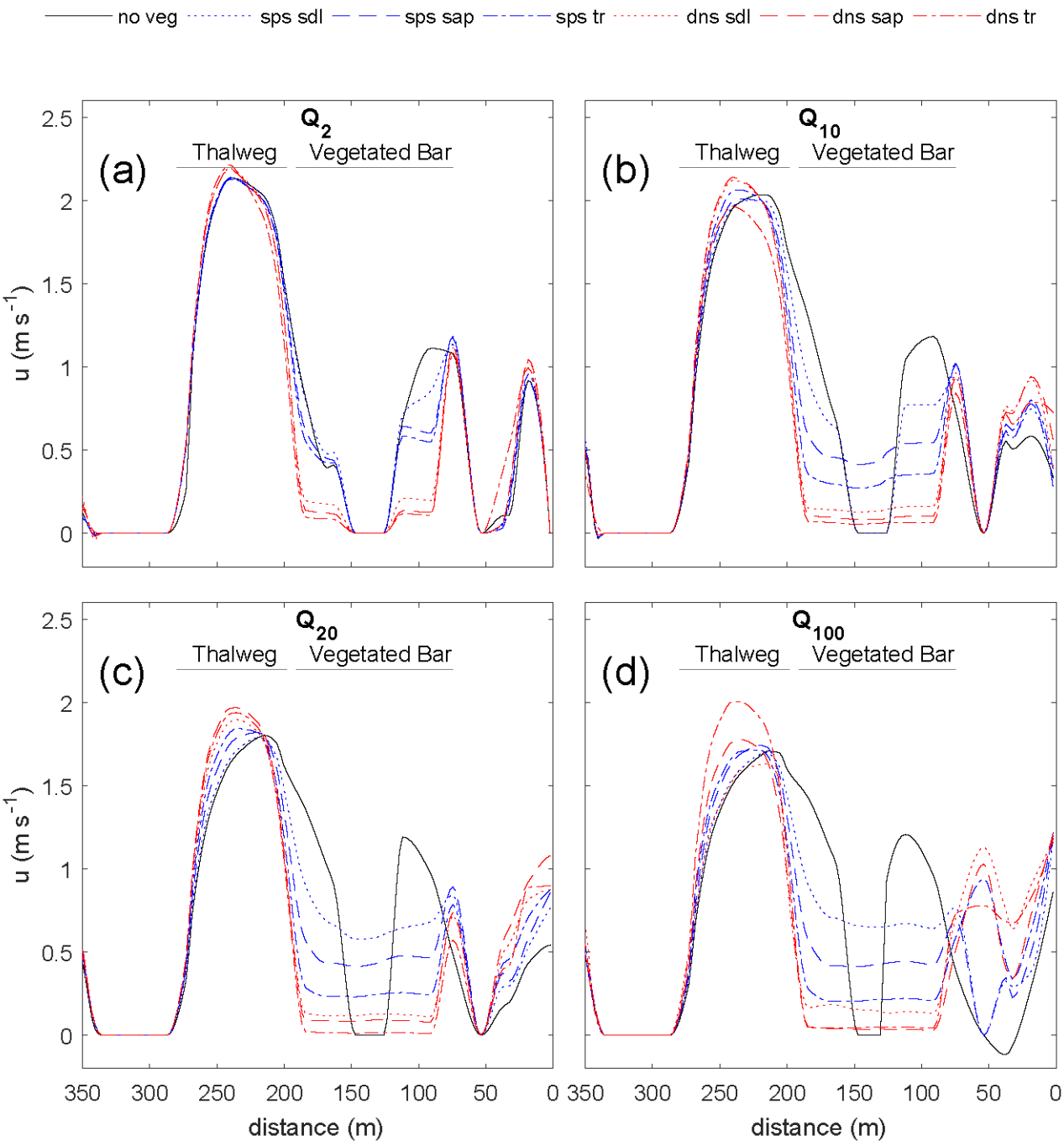
no veg
sps sdl
sps sap
sps tr
dns sdl
dns sap
dns tr
(a)
Q2
Thalweg
Vegetated Bar
(b)
Q10
Thalweg
Vegetated Bar
(c)
Q20
Thalweg
Vegetated Bar
(d)
Q100
Thalweg
Vegetated Bar
u (m s-1)
distance (m)
2.5
2
1.5
1
0.5
0
350
300
250
200
150
100
50
0

Figure 6. Effect of the vegetated bar ~~(j = 32–82)~~ on the streamwise (*u*) velocity at the midstream cross section (XS2) for the Q_2 (a), Q_{10} (b), Q_{20} (c), and Q_{100} (d) flows, with distance from river right end point (Figure 4). In the thalweg ~~(j = 100)~~, *u* increases and the maximum shifts toward the left bank. On the bar, velocity is decreased in the patch, and increased at the right edge of the patch.

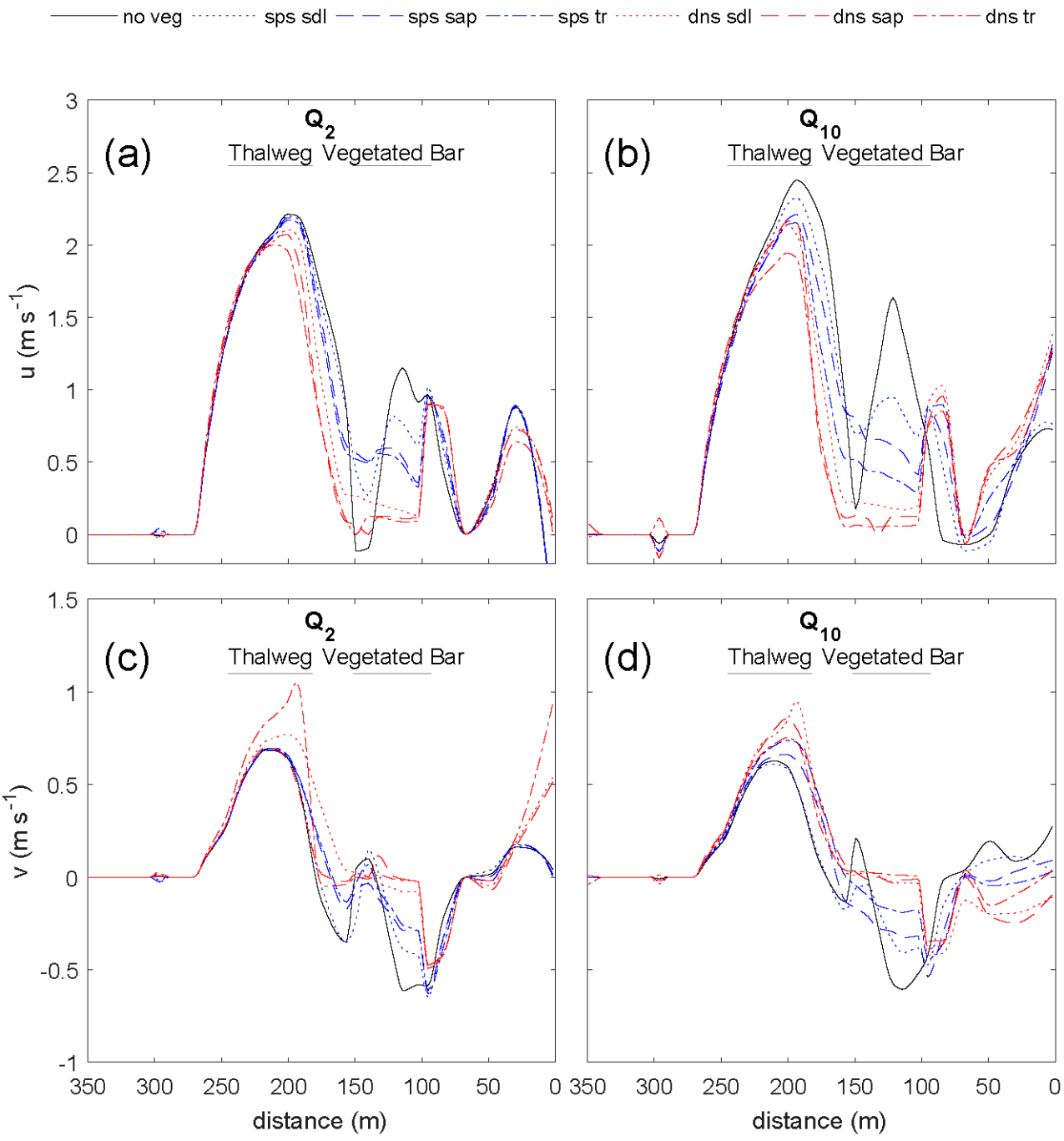
no veg
sps sdl
sps sap
sps tr
dns sdl
dns sap
dns tr
(a)
Q2
Thalweg Vegetated Bar
(b)
Q10
Thalweg Vegetated Bar
(c)
Q2
Thalweg Vegetated Bar
(d)
Q10
Thalweg Vegetated Bar
u (m s-1)
v (m s-1)
distance (m)
distance (m)

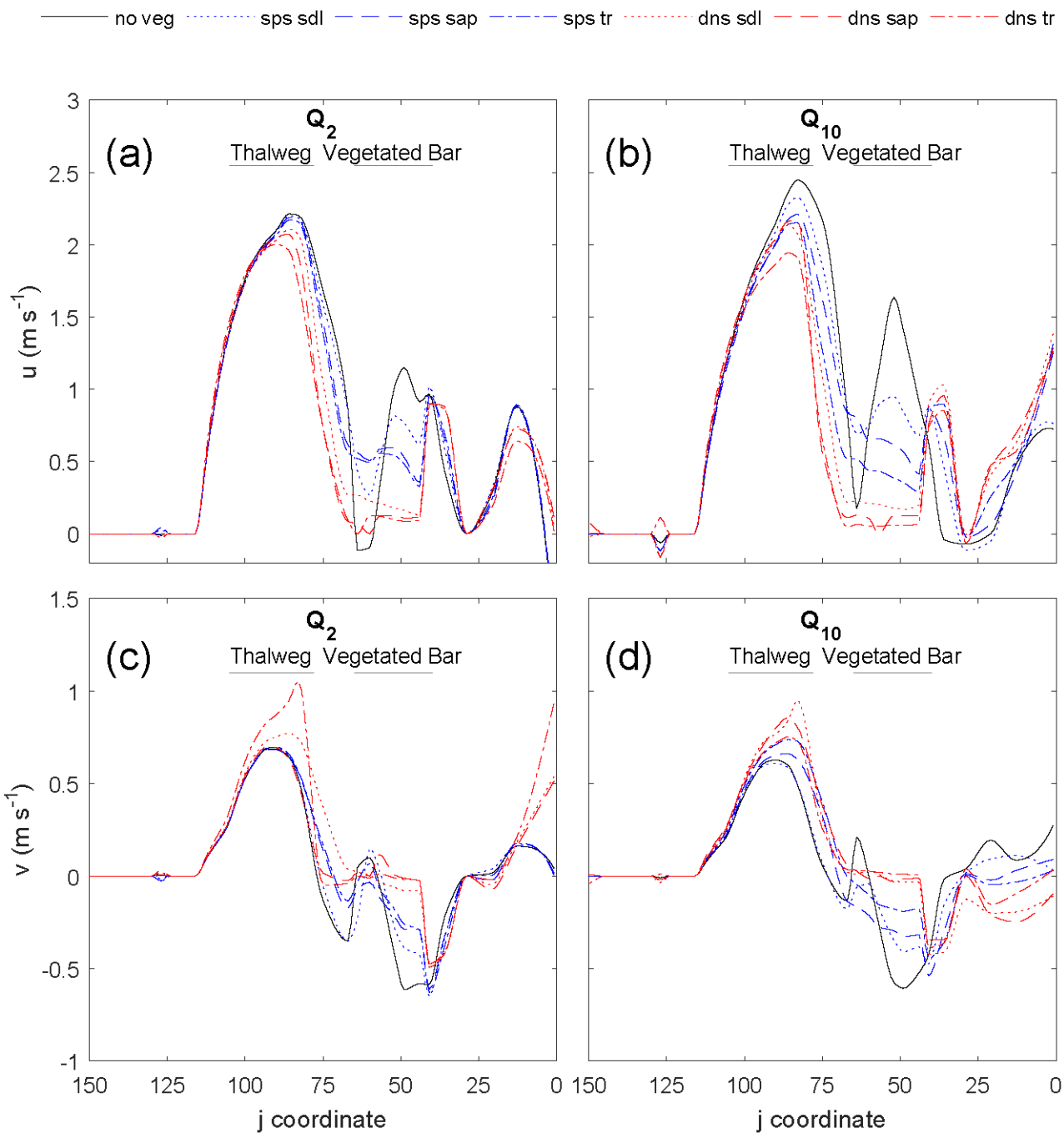

Figure 7. Effect of the vegetated bar ~~(j = 50–65)~~ on the streamwise (*u*; a,b) and stream-normal (*v*; c,d) velocity at the upstream cross section (XS1) for the Q_2 (a,c) and Q_{10} (b,d) flows, with distance from river right end point (Figure 4). In the thalweg ~~(j = 90)~~ and at

the head of the bar, *u* is decreased with increasing seedling size and density. For Q ≥ Q_{10}, *v* became more negative adjacent to the vegetation patch.

The manner in which different vegetation densities and growth stages influenced hydraulics varied spatially around the bend. In general, adding vegetation increased velocity within the thalweg and at the edge of the vegetation patch compared to the no-vegetation case, creating concentrated flow paths adjacent to the patch while reducing velocity and shear stress at the head of the bar and within the vegetation patch. The effect of the vegetated bar on channel-bend hydraulics became more pronounced with discharges increasing from the Q_2 to Q_{10}. Furthermore, sparse vegetation behaved similarly to the no-vegetation scenario for low flows, but had an increasing effect on hydraulics at the Q_{10}. Vegetation effects increased steeply from Q_2 to Q_{10} with modest changes thereafter. In general, hydraulics were more sensitive to plant morphology differences (A_c) for sparse conditions compared to dense conditions (Fig. 5, 6, 7).

At the downstream end of the bar (XS1; Fig. 5), vegetation increased the magnitude of downstream (*u*) and cross-stream (*v* more negative) velocity within the thalweg region, and reduced velocities over the bar. For flows ≥ $Q_{10,}$ the high-velocity core became more concentrated and shifted away from the bar. Results for the Q_{20} and Q_{100} flow were similar to that of the Q_{10} (Fig. S2). This thalweg effect became more pronounced with increasing plant density and plant size, except in the case of dense young trees, which behaved more similarly to the bare bar scenario for the Q_{10} flow. Amplification of thalweg velocities at XS1 was greatest for the dense sapling scenario, with 17 % and 12 % increases in *u* and *v*, respectively, for the $Q_{10,}$ and increases in velocity magnitude for flows > Q_{10}. On the vegetated bar, *u* and *v* decreased within the vegetated patch, with *u* values reduced up to 56 % for the sparse young tree scenario, and up to 95 % for the dense scenarios — these magnitudes are well above uncertainty in velocities. With increasing plant size and density, the values of *u* and *v* at the right edge of the vegetation patch were greater than or nearly equal to that in the thalweg, with a particularly large increase for dense scenarios. Thus, flow velocities were decreased within the patch, increased adjacent to the patch, and were deflected toward the left bank.

At the midstream position (XS2), downstream velocities (*u*) in the thalweg region were greater than at XS1. The impact of the vegetation patch on *u* for XS2 was pronounced, with *u* increased up to 30 % within the thalweg and the maximum value of *u* shifted toward the left bank with increasing plant size, density, and discharge (Fig. 6). Like XS1, the thalweg effect reached a maximum for dense saplings at the Q_{10}. As flow increased (Q_{20} and Q_{100}), dense trees had the greatest effect on increasing thalweg *u.* On the bar, the effect on *u* for XS2 was similar to XS1. Values of *u* decreased with increasing size and density of plants, and *u* increased at the right outer edge of the vegetation patch. Over the bar, *u* was reduced up to 99 % for the dense scenarios compared to the no-vegetation scenario, and increased at the edge of the patch up to 3300 %. At XS2, *v* values were small compared to XS1 and XS3 and were relatively insensitive to the presence of the vegetation patch (Fig. S3).

At the upstream end of the bar (XS3; Fig. 7), an opposite trend in changes in *u* within the thalweg was observed. With increasing seedling size and density, *u* was decreased within the thalweg and at the head of the bar, with a maximum reduction in *u* of 29 % for dense scenarios. Results for the Q_{20} and Q_{100} flow were similar to that of the Q_{10} (Fig. S4). For Q ≥ Q_{10}, *v* was more positive to the left (70 %) of the vegetation patch and within the thalweg and more negative to the right of the vegetation

patch ~~(180 % reduced)~~. Within the vegetation patch, u and v were reduced (96 % and 100 %, respectively). Thus, flow was steered away from the vegetation patch.

4 Discussion

4.1 Impact of vegetation on channel-bend hydraulics

Our results illustrate that vegetation enhances flow steering on bars, complementing previous work on bend dynamics in the absence of vegetation. Dietrich and Smith (1983) showed that bars steer flow in a manner that forces the high-velocity core toward the concave bank. They additionally found that flow over the heads of bars resulted in cross-stream components of velocity (v) and boundary shear stress (τ_n) directed toward the concave bank. Laboratory studies by Blanckaert (2010), representing sharp meander bends, ~~identified relationships between zones of inward versus outward mass transport, transverse bed profiles, and curvature variations, as well as~~ illustrat~~ed~~ing that curvature-induced secondary flow associated with topographic steering concentrates most discharge over the deepest, outer parts of a bend and influences bed topography via vertical, downwelling velocities that contribute to pool scour and inward, near-bed velocities that help maintain steep, transverse bed slopes. In our simulations, the presence of dense vegetation increased downstream velocity (u) within the thalweg up to 30 % and shifted the high-velocity core toward the cutbank, at the mid- and downstream sections of the channel bend investigated. Vegetation effects on cross-stream velocity (v) also illustrated flow steering toward the concave bank. Vegetation increased the magnitude of v at both the up- and downstream end of the channel bend, by increasing cross-stream flow toward the cutbank at the head of the bar and around the toe of the bar, where positive v values within the thalweg region at the upstream cross section show outward flow steering. By extension, cross-stream shear stress,is directed toward the concave bank. At the head of the bar, flow was additionally slowed within the channel (u decreased), and steered away from the vegetation patch, increasing flow within a side channel adjacent to the bar head and creating concentrated flow paths adjacent to the patch.

This modeling effort also contributes to evaluation of the stage-dependence of flow steering by bars. Whiting (1997) hypothesized that convective accelerations arising from flow steering would be most important at low flows, whereas Legleiter et al. (2011) showed that steering from bars continued to be important with increasing discharge. Our results suggest that flow steering will continue to be important over a range of flows for vegetated bars; i.e., vegetation effects on flow did not decrease with increasing discharge, consistent with Abu-Aly et al. (2014). We found that vegetation began to have a detectable impact on channel-bend hydraulics for flows greater than the Q_2, when plants were inundated, and that vegetation-induced alteration of hydraulics was initially steep from Q_2 to Q_{10}, with modest changes thereafter. ~~Vegetation effects on flow did not decrease with increasing discharge, consistent with Abu-Aly et al. (2014). Whereas flow steering from bars may be most important at low flows (Whiting, 1997), our results suggest that flow steering will continue to be important over a range of flows for vegetated bars.~~

In general, we found the impact of the vegetated bar on channel-bend hydraulics to vary with both plant density and morphology, and our modeling illustrated nuances in these relationships. Plant morphology differences affected hydraulics preferentially for sparse cases, whereas dense cases were similar. Dense young trees did not always result in the maximum alteration to channel-bend hydraulics—particularly for u during the Q_{10} flow. At the downstream end of the bar, the high-velocity core became more concentrated and shifted away from the bar with increasing plant density and plant size, except in the case of dense young trees. Dense young trees behaved more similarly to the bare bar scenario for the Q_{10}. This indicates there may be thresholds whereby increasing density and size of vegetation no longer results in an additional hydraulic effect in some cases. Together, these results suggest altered bend hydraulics caused by bar vegetation may be most pronounced for vegetation-inundating flows up to Q_{10} under sparse-vegetation conditions. We may expect vegetation-morphodynamic interactions to be strongest as recruited sparse woody riparian vegetation matures under moderate flow conditions ($> Q_2$ to Q_{10}), or conversely, if a bare bar establishes dense vegetation. This is consistent with the biogeomorphic phase concept (Corenblit et al., 2007, 2015a, 2015b), whereby established vegetation has strong feedbacks with geomorphic processes, but with the additional constraint of enhanced interactions under a specific range of flow magnitudes.

~~At the mid- and downstream sections of the channel bend investigated, the presence of dense vegetation increased downstream velocity (u) within the thalweg up to 30 % and shifted the high velocity core toward the cutbank. Vegetation increased the magnitude of cross-stream velocity (v) at both the up- and downstream end of the channel bend by increasing cross-stream flow toward the cutbank at the head of the bar and around the toe of the bar. Positive v values within the thalweg region at the upstream cross section (XS3) indicate, indeed, flow is steered toward the concave bank. By extension, cross-stream shear stress,is directed toward the concave bank. At the head of the bar, flow was additionally slowed within the channel (u decreased), and steered away from the vegetation patch, increasing flow within a side channel adjacent to the bar head and creating concentrated flow paths adjacent to the patch.~~

We acknowledge that some of our findings may be influenced by limitations of our modeling approach, which reflect persistent challenges in characterizing the complexities of vegetation architecture and flow in a modeling framework. Simplifications including representing plants as rigid cylinders (after Vargas-Luna et al., 2016) with a constant drag coefficient of 1 are ~~Our analysis simplified vegetation drag by assuming rigid cylinders, which has been found to be most accurate for dense vegetation (Vargas-Luna et al., 2016). We used a constant vegetation drag coefficient,~~ consistent with other studies but ~~. This approach~~ likely overestimate~~s~~ vegetation drag at higher discharges, when the canopy is inundated and plants are more streamlined, reducing A_c and $C_{d,v}$ (James et al., 2004). Future research directions include: 1) refining how vegetation drag is represented, especially for sparse vegetation; 2) quantifying changes in drag that result from streamlining and reconfiguration during inundation; 3) including variations in drag coefficient for vegetation to represent depth-dependence and complexities of vegetation architecture; and 4) evaluating effects of non-logarithmic vertical velocity structures (Aberle and Järvelä, 2013; Boothroyd et al., 2017; Nepf, 2012; Västilä et al., 2013; Västilä and Järvelä, 2014; Whittaker et al., 2013).

4.2 Implications for channel morphology and evolution

The reduction of velocity and shear stress within the thalweg at the bar head caused by the presence of the vegetated bar would be expected to decrease sediment transport in this region. Van Dijk et al. (2013), in an experimental channel, found bar vegetation to increase fine-sediment deposition upstream of the vegetation patch, analogous to the bar head of our work. This may contribute to bar-head maintenance, such that the head of the bar is not eroded. Maintenance of the bar head would be countered by the potential for chute cutoff (van Dijk et al., 2014) or channel switching that may result because of concentrated flow paths. Along the inside (river right) edge of the vegetated bar, a lower-elevation, chute-channel-like region is present, in which flow was concentrated and velocities increased as vegetation size and density increased. Seedling establishment was not successful in the lower-elevation region during the study period, possibly because higher shear stresses in this region limited fine sediment deposition conducive to recruitment and/or exceeded uprooting thresholds (Bywater-Reyes et al., 2015). The concentrated flow paths adjacent to the vegetation patch, on the inside of the bar, may be characteristic of conditions on vegetated bars along channel bends more generally, where both ridge and swale topography and chute bars may be present (Kleinhans and van den Berg, 2011), and where chute cutoffs and vegetation roughness and cohesion interact to influence morphodynamics (e.g., Braudrick et al., 2009). Seedlings often recruit along floodlines (Schnauder and Moggridge, 2009), forming rows of trees. Low-velocity areas within the rows induce fine-sediment deposition, steering flow away from the rows, and increasing velocity and shear stress adjacent to the rows such that sediment is transported in these regions. This process has been invoked to explain how vegetation creates vegetated islands (Gurnell et al., 2001), alternating patterns of vegetated ridges and adjacent channels (Tooth and Nanson, 2000), and the evolution of anabranching channels (Tooth et al., 2008). Van Dijk et al. (2013) found flood-dispersed vegetation recruited on bars resulted in island braiding, whereas vegetation distributed uniformly across the floodplain maintained a single-thread meandering channel with increased sinuosity and decreased bend wavelength. Our analysis, more comparable to the flood-dispersed case, shows the potential for development of vegetated islands, but also for ~~prevention~~ obstruction of chute cutoff through bar-head maintenance; chute cutoff may be more likely in the absence of vegetation (Constantine et al., 2010).

The production of a low-velocity region over the vegetated bar could increase fine-sediment deposition ~~on the bar~~, consistent with flume and field observations. Elevated sediment deposition within patches of woody seedlings, with variations depending on plant characteristics, has been documented in meandering (Kui et al., 2014) and straight (Diehl et al., 2017b) flumes. Gorrick and Rodríguez (2012), working in a flume in which vegetation patches were simulated with dowels, documented elevated fine-sediment deposition within the patches (Gorrick and Rodríguez, 2012). Zones of fine sediment deposition on bars associated with roughness from vegetation or instream wood can in turn create sites for plant germination and seedling growth (e.g., Gurnell and Petts, 2006). If reduced velocities result in increased deposition of sediment on the bar, bar accretion would induce additional topographic steering. This feedback would be expected to accelerate channel migration rates.

The increase in velocity and shift of the high velocity core toward the cutbank combined with low velocities within the vegetation patch would create a large velocity gradient across the channel. A larger velocity gradient within the thalweg compared to over the bar would be expected to alter the dynamics of bank erosion. Parker et al. (2011) propose that ~~A~~as a simple rule, bank erosion rate, $\dot{n}$, ~~according to Parker et al.'s (2011) HIPS model~~ is proportional to an erosion coefficient, k, and half the streamwise velocity difference between the two banks, Δu:

$$\dot{n} = k\Delta u \qquad (4)$$

The parameter, k, represents the material cohesion and vegetation root properties that control bank erosion and varies between 10^{-8} and 10^{-7} (dimensionless). For an assumed k, vegetation-induced velocity gradients across the channel are expected to alter bank erosion rates. ~~Thus, although we show the potential for concentrated flow paths to cause a morphology with vegetated islands, our analysis does not preclude bar vegetation from increasing bank erosion rates that would tend to increase sinuosity, in contrast to previous experimental work suggesting flood-established vegetation should result in island development (Van Dijk et al., 2013).~~

Vegetation "pushing" flow toward the outer bank is analogous to "bar push" (Allmendinger et al., 2005; Parker et al., 2011), whereby a rapidly accreting point bar may cause erosion at the outer bank (Eke et al., 2014; van de Lageweg et al., 2014). This increase in bank erosion would be countered by deposition of fine sediment on the bar resulting from the vegetation-induced reduction in velocity in this region, that may in turn induce additional "push" through bar building (e.g., Eke et al., 2014). Coarse bank roughness counters this effect, pushing the high--velocity core back toward the center of the channel (Gorrick and Rodríguez, 2012; Thorne and Furbish, 1995). The balance between erosion of the bank and deposition on the bar would thus dictate whether net erosion or net deposition within the active channel occurs, inducing changes in channel width (Eke et al., 2014), and altering channel morphology.

5 Conclusion

The presence of a vegetated bar in a gravel-bed river altered both streamwise and cross-stream components of velocity vectors for overbank flows, with an increasing effect with discharge and both plant density and size. Vegetation steered flow away from the vegetated bar, creating concentrated flow paths in surrounding low-elevation side channels and a low-velocity region over the vegetated patch. Flow was slowed at the apex of the bar, and increased within the thalweg around the bend. These changes in hydraulics could increase fine sediment deposition on the bar, potentially creating hospitable sites for vegetation recruitment, and increasing bank erosion that is dependent on cross-stream velocity gradients. This pattern would tend to reduce cross-stream sediment transport at the bar head, but increase it around the remainder of the bend.

Following the pattern of hydraulics, we would expect vegetation to change the morphodynamic evolution of channels with vegetation pushing flow in a manner typically attributed to bars, and increasing bank erosion rates. Bank retreat may induce bar building, which could be accelerated by fine-sediment deposition within the vegetation patch. This feedback would induce additional topographic steering from the presence of the bar. With a numerical model, we have characterized a

mechanisms by which channels with vegetated bars may evolve different morphologies and rates compared to those without, thereby contributing to understanding of ecogeomorphic feedbacks in river-floodplain systems (Gurnell, 2014) and of how life influences landscapes (Dietrich and Perron, 2006).

List of terms

A_c = vegetation frontal area (m^2)

C_d = channel drag coefficient

$C_{d,v}$ = vegetation drag coefficient

D = median grain size (m)

F_D = vegetation drag ($N\ m^{-2}$)

g = acceleration due to gravity ($m\ s^{-2}$)

k = bank erosion coefficient

u = streamwise component of velocity ($m\ s^{-1}$)

$\bar{U}$ = depth-averaged velocity ($m\ s^{-1}$)

U_x = x component of velocity in Cartesian coordinate system ($m\ s^{-1}$)

U_y = y component of boundary velocity in Cartesian coordinate system ($m\ s^{-1}$)

U_c = approach velocity ($m\ s^{-1}$)

v = stream-normal component of velocity ($m\ s^{-1}$)

ρ = density of water ($kg\ m^{-3}$)

ρ_s = density of sediment ($kg\ m^{-3}$)

τ = boundary shear stress ($N\ m^{-2}$)

τ^* = Shields number

n = stem density (#stems m^{-2})

$\dot{n}$ = bank erosion rate

Data availability

~~Please inquire with Missoula County for a~~Aerial LiDAR data used here are available from the Missoula County, Montana Geographic Information Systems office. Ground-based LiDAR is available at https://tls.unavco.org/projects/U-026/; Bitterroot Site 1 DOI: 10.7283/R34M07; Bitterroot Site 2 DOI: 10.7283/R30W61, Bitterroot Site 3 DOI: 10.7283/R3W62P. FaSTMECH solver files are available upon request.

Author contribution

S. Bywater-Reyes and A.C. Wilcox designed the modeling experiment. R.M. Diehl contributed to updating FaSTMECH code to account for vegetation drag. S. Bywater-Reyes carried out field work and model construction, calibration, and implementation. S. Bywater-Reyes wrote the manuscript with contributions from all co-authors.

Acknowledgements

This research was funded by the National Science Foundation (EAR-1024652, EPS-1101342) and EPA STAR Graduate Fellowship. We thank Mark Reiling, Philip Ramsey and MPG Ranch for access to the Bitterroot site. We thank Missoula County for providing LiDAR. We thank Sarah Doelger and UNAVCO, Austin Maphis, Katie Monaco, April Sawyer, and John Bowes for assistance in the field. A special thanks to Carl Legleiter for sharing his scripts and Richard McDonald, Gregory Pasternack, Daniele Tonina, David Machač, Nicholas Silverman, and Doug Brugger for modeling and scripting tips. The Mexcgns-Matlab scripts used in this study are available upon request of the first author.

Supplement

Supporting experimental procedures and additional results figures can be found in the supplement

References

Aberle, J. and Järvelä, J.: Flow resistance of emergent rigid and flexible floodplain vegetation, J. Hydraul. Res., 51(1), 33–45, doi:10.1080/00221686.2012.754795, 2013.

Abu-Aly, T. R., Pasternack, G. B., Wyrick, J. R., Barker, R., Massa, D. and Johnson, T.: Effects of LiDAR-derived, spatially distributed vegetation roughness on two-dimensional hydraulics in a gravel-cobble river at flows of 0.2 to 20 times bankfull, Geomorphology, 206, 468–482, doi:10.1016/j.geomorph.2013.10.017, 2014.

Allmendinger, N. E., Pizzuto, J. E., Potter, N., Johnson, T. E. and Hession, W. C.: The influence of riparian vegetation on stream width, eastern Pennsylvania, USA, Geol. Soc. Am. Bull., 117(1), 229–243, doi:10.1130/B25447.1, 2005.

Amlin, N. M. and Rood, S. B.: Comparative tolerances of riparian willows and cottonwoods to water-table decline, Wetlands, 22(2), 338–346, 2002.

Antonarakis, A. S., Richards, K. S., Brasington, J. and Muller, E.: Determining leaf area index and leafy tree roughness using terrestrial laser scanning, Water Resour. Res., 46(6), W06510, doi:10.1029/2009WR008318, 2010.

Asahi, K., Shimizu, Y., Nelson, J. and Parker, G.: Numerical simulation of river meandering with self-evolving banks, J. Geophys. Res. Earth Surf., 118(February), 1–22, doi:10.1002/jgrf.20150, 2013.

Baptist, M., Bosch, L. van den, Dijkstra, J. T. and Kapinga, S.: Modelling the effects of vegetation on flow and morphology in rivers, in Large Rivers, vol. 15, pp. 339–357, Arch. Hydrobiol., 2005.

Baptist, M., Babovic, V., Rodríguez, J., Keijzer, M., Uittenbogaard, R., Mynett, A. and Verwey, A.: On inducing equations for vegetation resistance, J. Hydraul. Res., 45(4), 435–450, 2007.

Bendix, J. and Hupp, C.: Hydrological and geomorphological impacts on riparian plant communities, Hydrol. Process., 14, 2977–2990, 2000.

Bennett, S. J., Pirim, T. and Barkdoll, B. D.: Using simulated emergent vegetation to alter stream flow direction within a straight experimental channel, Geomorphology, 44(1–2), 115–126, 2002.

Bertoldi, W. and Siviglia, A.: Modeling vegetation controls on fluvial morphological trajectories, Geophys. Res. Lett., 41, 1–9, doi:10.1002/2014GL061666, 2014.

Blanckaert, K.: Topographic steering, flow recirculation, velocity redistribution, and bed topography in sharp meander bends, Water Resour. Res., 46(9), 1–23, doi:10.1029/2009WR008303, 2010.

Blondeaux, P. and Seminara, G.: A unified bar-bend theory of river meanders, J. Fluid Mech., 157, 449–470, 1985.

Boothroyd, R. J., Hardy, R. J., Warburton, J. and Marjoribanks, T. I.: The importance of accurately representing submerged vegetation morphology in the numerical prediction of complex river flow, Earth Surf. Process. Landforms, 41, 567–576, doi:10.1002/esp.3871, 2016.

Boothroyd, R. J., Hardy, R. J., Warburton, J. and Marjoribanks, T. I.: Modeling complex flow structures and drag around a submerged plant of varied posture, Water Resour. Res., 53, 2877–2901, doi:10.1002/2016WR020186, 2017.

Boyd, K., Thatcher, T. and Kellogg, W.: Musselshell River Watershed Plan, , (September), 131, 2015.

Braudrick, C. A., Dietrich, W. E., Leverich, G. T. and Sklar, L. S.: Experimental evidence for the conditions necessary to sustain meandering in coarse-bedded rivers., Proc. Natl. Acad. Sci. U. S. A., 106(40), 16936–41, doi:10.1073/pnas.0909417106, 2009.

Bywater-Reyes, S., Wilcox, A. C., Stella, J. C. and Lightbody, A. F.: Flow and scour constraints on uprooting of pioneer woody seedlings, Water Resour. Res., 51(11), 9190–9206, doi:10.1002/2014WR016641, 2015.

Bywater-Reyes, S., Wilcox, A. C. and Diehl, R. M.: Multiscale influence of woody riparian vegetation on fluvial topography quantified with ground-based and airborne lidar, J. Geophys. Res. Earth Surf., 122(6), 1218–1235, doi:10.1002/2016JF004058, 2017.

Camporeale, C., Perucca, E., Ridolfi, L. and Gurnell, A.: Modeling the interactions between river morphodynamics and riparian vegetation, Rev. Geophys., 51, 1–36, doi:10.1002/rog.20014, 2013.

Constantine, J. A., McLean, S. R. and Dunne, T.: A mechanism of chute cutoff along large meandering rivers with uniform floodplain topography, Geol. Soc. Am. Bull., 122, 855–869, doi:10.1130/B26560.1, 2010.

Corenblit, D., Tabacchi, E., Steiger, J. and Gurnell, A. M.: Reciprocal interactions and adjustments between fluvial landforms and vegetation dynamics in river corridors: A review of complementary approaches, Earth-Science Rev., 84, 56–86, doi:10.1016/j.earscirev.2007.05.004, 2007.

Corenblit, D., Davies, N. S., Steiger, J., Gibling, M. R. and Bornette, G.: Considering river structure and stability in the light of evolution: feedbacks between riparian vegetation and hydrogeomorphology, Earth Surf. Process. Landforms, 40(September 2014), 189–207, doi:10.1002/esp.3643, 2015a.

Corenblit, D., Baas, A., Balke, T., Bouma, T., Fromard, F., Garófano-Gómez, V., González, E., Gurnell, A. M., Hortobágyi, B., Julien, F., Kim, D., Lambs, L., Stallins, J. A., Steiger, J., Tabacchi, E. and Walcker, R.: Engineer pioneer plants respond to and affect geomorphic constraints similarly along water-terrestrial interfaces world-wide, Glob. Ecol. Biogeogr., 1–14, doi:10.1111/geb.12373, 2015b.

Curran, J. C. and Hession, W. C.: Vegetative impacts on hydraulics and sediment processes across the fluvial system, J. Hydrol., 505, 364–376, doi:10.1016/j.jhydrol.2013.10.013, 2013.

Dean, D. J. and Schmidt, J. C.: The role of feedback mechanisms in historic channel changes of the lower Rio Grande in the Big Bend region, Geomorphology, 126, 333–349, doi:10.1016/j.geomorph.2010.03.009, 2011.

Diehl, R. M., Merritt, D. M., Wilcox, A. C. and Scott, M. L.: Applying functional traits to ecogeomorphic processes in riparian ecosystems, Bioscience, 67(8), 729–743, doi:10.1093/biosci/bix080, 2017a.

Diehl, R. M., Wilcox, A. C., Stella, J. C., Kui, L., Sklar, L. S. and Lightbody, A.: Fluvial sediment supply and pioneer woody seedlings as a

control on bar-surface topography, Earth Surf. Process. Landforms, 42(5), 724–734, doi:10.1002/esp.4017, 2017b.

Dietrich, W. E. and Perron, J. T.: The search for a topographic signature of life, Nature, 439, 411–418, doi:10.1038/nature04452, 2006.

Dietrich, W. E. and Smith, J. D.: Influence of the point bar on flow through curved channels, Water Resour. Res., 19(5), 1173–1192, 1983.

Dietrich, W. E. and Whiting, P.: Boundary shear stress and sediment transport in river meanders of sand and gravel, in River Meandering. AGU Water Resources Monograph 12, edited by S. Ikeda and G. Parker, pp. 1–50, American Geophysical Union, Washington DC., 1989.

van Dijk, W. M., Schuurman, F., van de Lageweg, W. I. and Kleinhans, M. G.: Bifurcation instability and chute cutoff development in meandering gravel-bed rivers, Geomorphology, 213, 277–291, doi:10.1016/j.geomorph.2014.01.018, 2014.

Van Dijk, W. M., Teske, R., Van De Lageweg, W. I. and Kleinhans, M. G.: Effects of vegetation distribution on experimental river channel dynamics, Water Resour. Res., 49(11), 7558–7574, doi:10.1002/2013WR013574, 2013.

Eke, E., Parker, G. and Shimizu, Y.: Numerical modeling of erosional and depositional bank processes in migrating river bends with self-formed width: Morphodynamics of bar push and bank pull, J. Geophys. Res. Earth Surf., 119, 1455–1483, doi:10.1002/2013JF003020, 2014.

Gorrick, S. and Rodríguez, J. F.: Sediment dynamics in a sand bed stream with riparian vegetation, Water Resour. Res., 48(2), 1–15, doi:10.1029/2011WR011030, 2012.

Gran, K. and Paola, C.: Riparian vegetation controls on braided stream dynamics, Water Resour. Res., 37(12), 3275–3283 [online] Available from: http://nced.umn.edu/system/files/2010sicm_gran2001.pdf (Accessed 2 February 2012), 2001.

Green, J. C.: Modelling flow resistance in vegetated streams: Review and development of new theory, Hydrol. Process., 19, 1245–1259, doi:10.1002/hyp.5564, 2005.

Gurnell, A.: Plants as river system engineers, Earth Surf. Process. Landforms, 39, 4–25, doi:10.1002/esp.3397, 2014.

Gurnell, A. and Petts, G.: Trees as riparian engineers: the Tagliamento River, Italy, Earth Surf. Process. Landforms, 1574(May), 1558–1574, doi:10.1002/esp, 2006.

Gurnell, A. M., Petts, G. E., Hannah, D. M., Smith, B. P. G., Edwards, P. J., Kollmann, J., Ward, J. V. and Tockner, K.: Riparian vegetation and island formation along the gravel-bed Fiume Tagliamento, Italy, Earth Surf. Process. Landforms, 26(1), 31–62, doi:10.1002/1096-9837(200101)26:1<31::AID-ESP155>3.0.CO;2-Y, 2001.

Ikeda, S., Parker, G. and Sawai, K.: Bend theory of river meanders. Part 1. Linear development, J. Fluid Mech., 112, 363–377, doi:10.1017/S0022112081000451, 1981.

Iwasaki, T., Shimizu, Y. and Kimura, I.: Numerical simulation of bar and bank erosion in a vegetated floodplain: A case study in the Otofuke River, Adv. Water Resour., doi:10.1016/j.advwatres.2015.02.001, 2015.

Jalonen, J., Järvelä, J. and Aberle, J.: Leaf area index as vegetation density measure for hydraulic analyses, J. Hydraul. Eng., 139(5), 461–469, doi:10.1061/(ASCE)HY.1943-7900.0000700, 2013.

James, C., Birkhead, A. and Jordanova, A.: Flow resistance of emergent vegetation, J. Hydraul. Res., 42(4), 37–41, 2004.

Karrenberg, S., Edwards, P. and Kollmann, J.: The life history of Salicaceae living in the active zone of floodplains, Freshw. Biol., 47(4), 733–748, 2002.

Kleinhans, M. G. and van den Berg, J. H.: River channel and bar patterns explained and predicted by an empirical and a physics-based method, Earth Surf. Process. Landforms, 36(6), 721–738, doi:10.1002/esp.2090, 2011.

Kui, L., Stella, J., Lightbody, A. and Wilcox, A. C.: Ecogeomorphic feedbacks and flood loss of riparian tree seedlings in meandering channel experiments, Water Resour. Res., 50, 9366–9384, doi:10.1002/2014WR015719., 2014.

van de Lageweg, W. I., van Dijk, W. M., Baar, a. W., Rutten, J. and Kleinhans, M. G.: Bank pull or bar push: What drives scroll-bar formation in meandering rivers?, Geology, 42(4), 319–322, doi:10.1130/G35192.1, 2014.

Legleiter, C. J., Harrison, L. R. and Dunne, T.: Effect of point bar development on the local force balance governing flow in a simple, meandering gravel bed river, J. Geophys. Res., 116(F1), F01005, doi:10.1029/2010JF001838, 2011.

Lightbody, A., Skorko, K., Kui, L., Stella, J. . and Wilcox, A. .: Hydraulic and topographic response of sand-bed rivers to woody riparian seedlings: field-scale laboratory methods and results, in 2012 Fall Meeting, AGU, San Fransisco, Calif., 3-7 Dec., vol. Abstract E, San Fransisco., 2012.

Manners, R., Schmidt, J. and Wheaton, J. M.: Multiscalar model for the determination of spatially explicit riparian vegetation roughness, J. Geophys. Res. Earth Surf., 118(1), 65–83, doi:10.1029/2011JF002188, 2013.

Manners, R. B., Wilcox, A. C., Kui, L., Lightbody, A. F., Stella, J. C. and Sklar, L. S.: When do plants modify fluvial processes? Plant-hydraulic interactions under variable flow and sediment supply rates, J. Geophys. Res. Earth Surf., 120(2), 325–345, doi:10.1002/2014JF003265, 2015.

Marjoribanks, T. I., Hardy, R. J., Lane, S. N. and Tancock, M. J.: Patch-scale representation of vegetation within hydraulic models, Earth Surf. Process. Landforms, 42(5), 699–710, doi:10.1002/esp.4015, 2017.

Mueller, E. R. and Pitlick, J.: Sediment supply and channel morphology in mountain river systems: 2. Single thread to braided transitions, J. Geophys. Res. Earth Surf., 119(7), 1516–1541, doi:10.1002/2013JF003045, 2014.

Murray, A. B. and Paola, C.: Modelling the effect of vegetation on channel pattern in bedload rivers, Earth Surf. Process. Landforms, 28(2), 131–143, doi:10.1002/esp.428, 2003.

Nelson, J. M.: iRIC Software: FaSTMECH solver manual, , 1–36, 2013.

Nelson, J. M. and Smith, J. D.: Flow in meandering channels with natural topography, in River Meandering, Water Resour. Monogr., vol. 12, edited by S. Ikeda and G. Parker, pp. 69–102, AGU, Washington DC., 1989.

Nelson, J. M., Bennett, J. P. and Wiele, S. M.: Flow and sediment-transport modeling, in Tools in Fluvial Geomorphology, edited by G. M. Kondolf and H. Piégay, pp. 539–576, Wiley, Chichester., 2003.

Nelson, J. M., Shimizu, Y., Abe, T., Asahi, K., Gamou, M., Inoue, T., Iwasaki, T., Kakinuma, T., Kawamura, S., Kimura, I., Kyuka, T., McDonald, R. R., Nabi, M., Nakatsugawa, M., Simões, F. R., Takebayashi, H. and Watanabe, Y.: The international river interface cooperative: Public domain flow and morphodynamics software for education and applications, Adv. Water Resour., 93, 62–74, doi:10.1016/j.advwatres.2015.09.017, 2016.

Nepf, H., Rominger, J. and Zong, L.: Coherent flow structures in vegetated channels, in Coherent Flow Structures at Earth's Surface, edited by J. G. Venditti, J. L. Best, M. Church, and R. J. Hardy, pp. 135–147, Wiley-Blackwell., 2013.

Nepf, H. M.: Drag, turbulence, and diffusion in flow through emergent vegetation, Water Resour. Res., 35(2), 479–489, doi:10.1029/1998WR900069, 1999.

Nepf, H. M.: Hydrodynamics of vegetated channels, J. Hydraul. Res., 503(3), 262–279, doi:10.1080/00221686.2012.696559, 2012.

Nicholas, A. P., Ashworth, P. J., Sambrook Smith, G. H. and Sandbach, S. D.: Numerical simulation of bar and island morphodynamics in anabranching megarivers, J. Geophys. Res. Earth Surf., 118, 1–26, doi:10.1002/jgrf.20132, 2013.

van Oorschot, M., Kleinhans, M., Geerling, G. and Middelkoop, H.: Distinct patterns of interaction between vegetation and morphodynamics, Earth Surf. Process. Landforms, 41(6), 791–808, doi:10.1002/esp.3864, 2016.

Osterkamp, W. R. and Hupp, C. R.: Fluvial processes and vegetation — Glimpses of the past, the present, and perhaps the future, Geomorphology, 116(3–4), 274–285, doi:10.1016/j.geomorph.2009.11.018, 2010.

Osterkamp, W. R., Hupp, C. R. and Stoffel, M.: The interactions between vegetation and erosion: New directions for research at the interface of ecology and geomorphology, Earth Surf. Process. Landforms, 37, 23–36, doi:10.1002/esp.2173, 2012.

Parker, G., Shimizu, Y., Wilkerson, G. V., Eke, E. C., Abad, J. D., Lauer, J. W., Paola, C., Dietrich, W. E. and Voller, V. R.: A new framework for modeling the migration of meandering rivers, Earth Surf. Process. Landforms, 36(1), 70–86, doi:10.1002/esp.2113, 2011.

Pasternack, G. B.: 2D modeling and ecohydraulic analysis, University of California at Davis., 2011.

Rominger, J. T., Lightbody, A. F., Nepf, H. M. and others: Effects of added vegetation on sand bar stability and stream hydrodynamics, J. Hydraul. Eng., 136(12), 994–1002, doi:10.1061/?ASCE?HY.1943-7900.0000215, 2010.

Rood, S. B., Kalischuk, A. R. and Mahoney, J. M.: Initial cottonwood seedling recruitment following the flood of the century of the Oldman River, Alberta, Canada, Wetlands, 18(4), 557–570, 1998.

Schnauder, I. and Moggridge, H. L.: Vegetation and hydraulic-morphological interactions at the individual plant, patch and channel scale, Aquat. Sci., 71(3), 318–330, doi:10.1007/s00027-009-9202-6, 2009.

Segura, C. and Pitlick, J.: Coupling fluvial-hydraulic models to predict gravel transport in spatially variable flows, J. Geophys. Res. Earth Surf., 120, 834–855, doi:10.1002/2014JF003302, 2015.

Straatsma, M. W., Warmink, J. J. and Middelkoop, H.: Two novel methods for field measurements of hydrodynamic density of floodplain vegetation using terrestrial laser scanning and digital parallel photography, Int. J. Remote Sens., 29(5), 1595–1617, doi:10.1080/01431160701736455, 2008.

Termini, D.: Experimental analysis of the effect of vegetation on flow and bed shear stress distribution in high-curvature bends, Geomorphology, 274, 1–10, doi:10.1016/j.geomorph.2016.08.031, 2016.

Thorne, S. D. and Furbish, D. J.: Influences of coarse bank roughness on flow within a sharply curved river bend, Geomorphology, 12(3), 241–257, doi:10.1016/0169-555X(95)00007-R, 1995.

Tonina, D. and Jorde, K.: Hydraulic modeling approaches for ecohydraulic studies: 3D , 2D , 1D and non-numerical models, in Ecohydraulics: An Integrated Approach, pp. 31–74., 2013.

Tooth, S. and Nanson, G. C.: The role of vegetation in the formation of anabranching channels in an ephemeral river, Northern plains, arid central Australia, Hydrol. Process., 3117(May 1999), 3099–3117 [online] Available from: http://onlinelibrary.wiley.com/doi/10.1002/1099-1085(200011/12)14:16/17%3C3099::AID-HYP136%3E3.0.CO;2-4/abstract (Accessed 2 February 2012), 2000.

Tooth, S., Jansen, J. D., Nanson, G. C., Coulthard, T. J. and Pietsch, T.: Riparian vegetation and the late Holocene development of an anabranching river: Magela Creek, northern Australia, Geol. Soc. Am. Bull., 120(7–8), 1021–1035, doi:10.1130/B26165.1, 2008.

Vargas-Luna, A., Crosato, A. and Uijttewaal, W. S. J.: Effects of vegetation on flow and sediment transport: Comparative analyses and validation of predicting models, Earth Surf. Process. Landforms, 40, 157–176, doi:10.1002/esp.3633, 2015.

Vargas-Luna, A., Crosato, A., Calvani, G. and Uijttewaal, W. S. J.: Representing plants as rigid cylinders in experiments and models, Adv. Water Resour., 93, 205–222, doi:10.1016/j.advwatres.2015.10.004, 2016.

Västilä, K. and Järvelä, J.: Modeling the flow resistance of woody vegetation using physically-based properties of the foliage and stem, Water Resour. Res., 50, 1–17, doi:10.1002/2013WR013819, 2014.

Västilä, K., Järvelä, J. and Aberle, J.: Characteristic reference areas for estimating flow resistance of natural foliated vegetation, J. Hydrol., 492, 49–60, doi:10.1016/j.jhydrol.2013.04.015, 2013.

Wang, C., Wang, Q., Meire, D., Ma, W., Wu, C., Meng, Z., Van de Koppel, J., Troch, P., Verhoeven, R., De Mulder, T. and Temmerman, S.: Biogeomorphic feedback between plant growth and flooding causes alternative stable states in an experimental floodplain, Adv. Water Resour., 93, 223–235, doi:10.1016/j.advwatres.2015.07.003, 2016.

Whiting, P. J.: The effect of stage on flow and components of the local force balance, Earth Surf. Process. Landforms, 22(6), 517–530, doi:10.1002/(SICI)1096-9837(199706)22:6<517::AID-ESP707>3.0.CO;2-M, 1997.

Whittaker, P., Wilson, C., Aberle, J., Rauch, H. P. and Xavier, P.: A drag force model to incorporate the reconfiguration of full-scale riparian trees under hydrodynamic loading, J. Hydraul. Res., 51(5), 569–580, doi:10.1080/00221686.2013.822936, 2013.

Wilcox, A. C. and Shafroth, P. B.: Coupled hydrogeomorphic and woody-seedling responses to controlled flood releases in a dryland river, Water Resour. Res., 49(April), n/a-n/a, doi:10.1002/wrcr.20256, 2013.

Wintenberger, C. L., Rodrigues, S., Bréhéret, J.-G. and Villar, M.: Fluvial islands: First stage of development from nonmigrating (forced) bars and woody-vegetation interactions, Geomorphology, 246, 305–320, doi:10.1016/j.geomorph.2015.06.026, 2015.

Yager, E. M. and Schmeeckle, M. W.: The influence of vegetation on turbulence and bed load transport, J. Geophys. Res. Earth Surf., 118(3), 1585–1601, doi:10.1002/jgrf.20085, 2013.

Supplement

Channel topography and model grid

LiDAR was flown by Watershed Sciences, Inc. (now Quantum Spatial) for Missoula County on October 30, 2012 with a Leica ALS60 with 3.83 ground points/m^2, providing 1-m resolution topography with a RMSE of 0.03 m. Inundated regions (reflected off water) were manually removed. In-channel bathymetry was measured with RTK-GPS cross-section surveys (Trimble R7 and 5800 with Trimble 5700 base station) augmented by Sonarmite echosounder measurements in non-wadeable areas. Monuments used for the LiDAR survey were occupied with the RTK GPS. Horizontal and vertical agreement of < 0.10 m was found. RTK topographic points were interpolated in the downstream direction, as is appropriate in rivers. RTK point density was 1.25 pts m^{-2}. All topographic points were combined in iRIC, from which we made ~~and a~~ a curvilinear orthogonal grid with a centerline following the general pattern of the channel over the model domain ~~created~~ with an average cell size of 2.5 by 2.5 m for calibration runs, and 5 by 5 m for the remaining runs, with corresponding 841,851 and 210,926 nodes, respectively. ~~The grid size was constant for the whole domain. We were unable to maintain a curvilinear, channel-fitted grid (nodes overlapped) so w~~We projected ~~our~~ Cartesian coordinate flow solution output to the nearest grid cell of a curvilinear grid (2 by 2 m average grid resolution) covering the channel bend of interest (Figure 3)~~main channel~~, and converted the associated output to streamwise and stream-normal values with a rotation matrix. A piecewise Cubic Hermite Interpolating Polynomial algorithm was applied to reduce artifacts from the transformation.

Model calibration

We surveyed water surface elevation (WSE) with RTK GPS in at least 30 WSE locations per calibration over a 180 m reach length for each calibration flow (see main text). The calibrated runs (Table 1; Fig. S1) had RMSE of 0.11 – to 0.18 m.

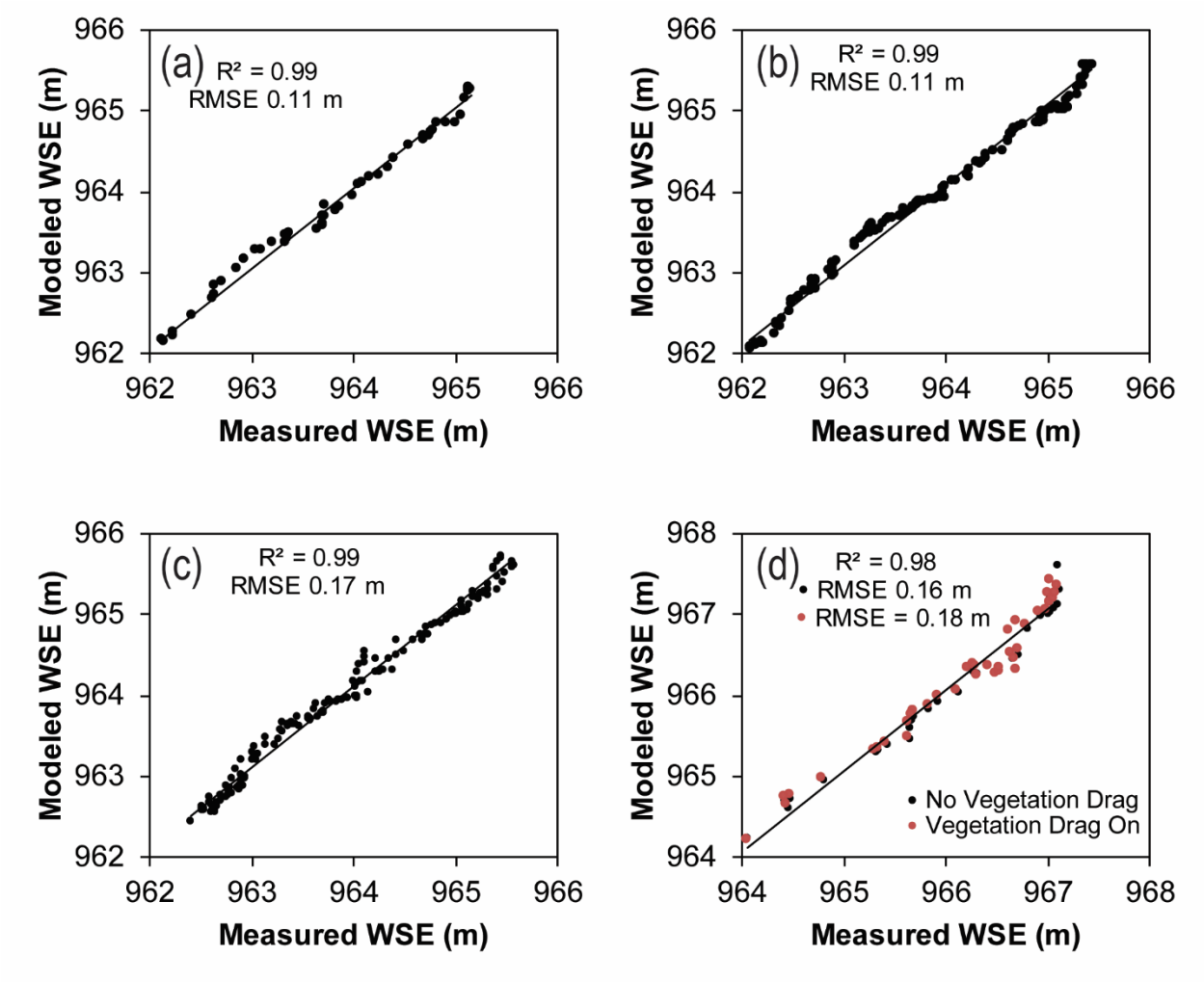

Figure S1. Water surface elevation (WSE) calibration for runs run 1 (a), 2 (b), 3 (c), 4 and 5 (d) (Table 1).

Velocity was measured during base flow in 2015 along cross sections in locations where little geomorphic change was observed following topography collection (Fig. 1) using a Teledyne RD Instruments (TRDI) four beam 1200 kHz Rio Grande ADCP mounted to a 12-ft cataraft equipped with rapid RTK GPS rowed manually. Data were collected using single ping

ensembles with Bottom Mode 12 and Water Mode 7, similar to the methods described in Rennie and Millar (2004), Rennie and Church (2010), and Venditti et al. (2015). Vertical velocity resolution was 0.25 m, with a minimum of four measurements. Velocities from the top 0.5 m and bottom 6 % of the depth were excluded. Velocities were corrected for boat speed with WinRiver II software using bottom tracking. Bed conditions were immobile, so additional corrections were not necessary.

Because velocity profiles were incomplete, data were exported in text format from WinRiver II, and each ensemble post-processed for depth-averaged velocity ($\bar{U}$) in Matlab R2012a by regressing velocity (U) as a function of log of height above the bed (z) to determine shear velocity (u^*) and roughness height (z_o) (Bergeron and Abrahams, 1992). Since U varies as a function of z:

$$U = \frac{u_*}{\kappa} \ln(\frac{z}{z_o}) \qquad \text{(S1)}$$

where κ is the von Karman constant (0.41), the regression of U as a function of z (Uz) yields:

$$U = m_{Uz} \ln(z) + c_{Uz} \qquad \text{(S2)}$$

where m_{Uz} is slope and c_{Uz} the intercept. Shear velocity, $u_{*_{Uz}}$, and roughness height, $z_{o_{Uz}}$, were calculated from the regression coefficients:

$$u_{*_{Uz}} = \kappa m_{Uz} \qquad \text{(S3)}$$

$$z_{o_{Uz}} = \exp(-c_{Uz}/m_{Uz}) \qquad \text{(S4)}$$

Using the law of the wall and our calculated $u_{*_{Uz}}$ and $z_{o_{Uz}}$, we calculated $\bar{U}$ for each ensemble assuming z_m = 0.37H, where H is the total depth:

$$\bar{U} = \frac{u_{*_{Uz}}}{\kappa} \ln(\frac{z_m}{z_{o_{Uz}}}) \qquad \text{(S5)}$$

Individual ensembles are noisy (e.g., Rennie and Church, 2010) and we wished to compare measured $\bar{U}$ to modeled $\bar{U}$. Thus we gridded measured velocities to match model output, ensuring grid cells were concurrent and orthogonal, and calculated the root mean square error (RMSE). We compared the RMSE of law-of-the-wall-derived $\bar{U}$ to a simple average assuming missing values for the top 0.5 m in each ensemble were equal to the value of U corresponding to the largest z. Law-of-the-wall-derived $\bar{U}$ had a lower RMSE, and was thus used instead of the adjusted average (RMSE 0.24 m s^{-1} compared to 0.33 m s^{-1}).

Floodplain vegetation

Individual floodplain trees were mapped (Fig. 1) from the airborne LiDAR, from which vegetation density (#stems m^{-2}), height (m) and diameter (m) were extracted. Vegetation points were isolated and ground vegetation removed with CloudCompare (http://www.danielgm.net/cc/). The dataset was imported as a las dataset in ArcGIS 10.1 and a 1-m resolution raster of maximum height created. Crowns were mapped following a workflow similar to Koch et al. (2006) in ArcGIS 10.1, whereby points were inverted and crowns delineated in a manner similar to delineating drainage basins, and the maximum height for each crown extracted as "basin" minima. Crown "basins" were converted to polygons. Method performance was evaluated by comparing crown polygons to aerial imagery. Nearly every tree large enough to be captured by the LiDAR was accurate (<5 % false positive). Crown attributes (centroid, area, and radius) were calculated using the field calculator. Height of each crown was determined by intersecting centroids with the height raster. Diameter at breast height for each tree was estimated by assuming a crown-diameter to stem-diameter relationship (Hemery et al.,

2005). Although this is a rough estimate, results were reasonable (mean diameter at breast height of 0.20 ± 0.14 m standard deviation).

Vegetation polygons were created by constructing a 15-m bounding polygon. The polygons were smoothed, gaps removed, and dissolved into a single polygon for each region. Average polygon attributes were calculated (vegetation density (#stems m^{-2}), height (m), diameter (m), and A_C (average flow depth multiplied by average diameter at breast height; m^2 per plant).

Supplemental results figures

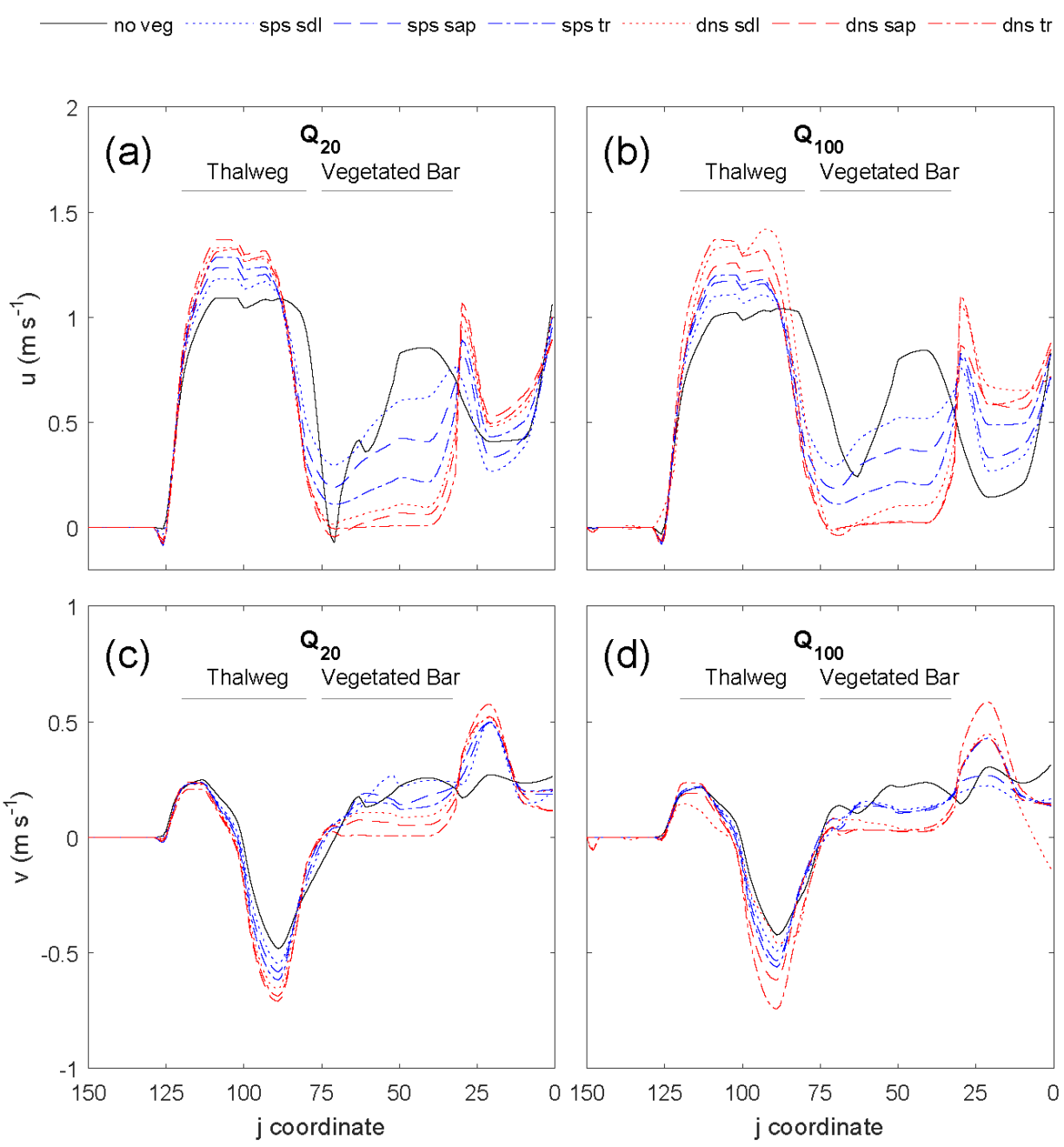
no veg
sps sdl
sps sap
sps tr
dns sdl
dns sap
dns tr
(a)
Q_{20}
Thalweg
Vegetated Bar
(b)
Q_{100}
Thalweg
Vegetated Bar
(c)
Q_{20}
Thalweg
Vegetated Bar
(d)
Q_{100}
Thalweg
Vegetated Bar
u (m s^{-1})
v (m s^{-1})
2
1.5
1
0.5
0
1
0.5
0
-0.5
-1
150
125
100
75
50
25
0
j coordinate

86

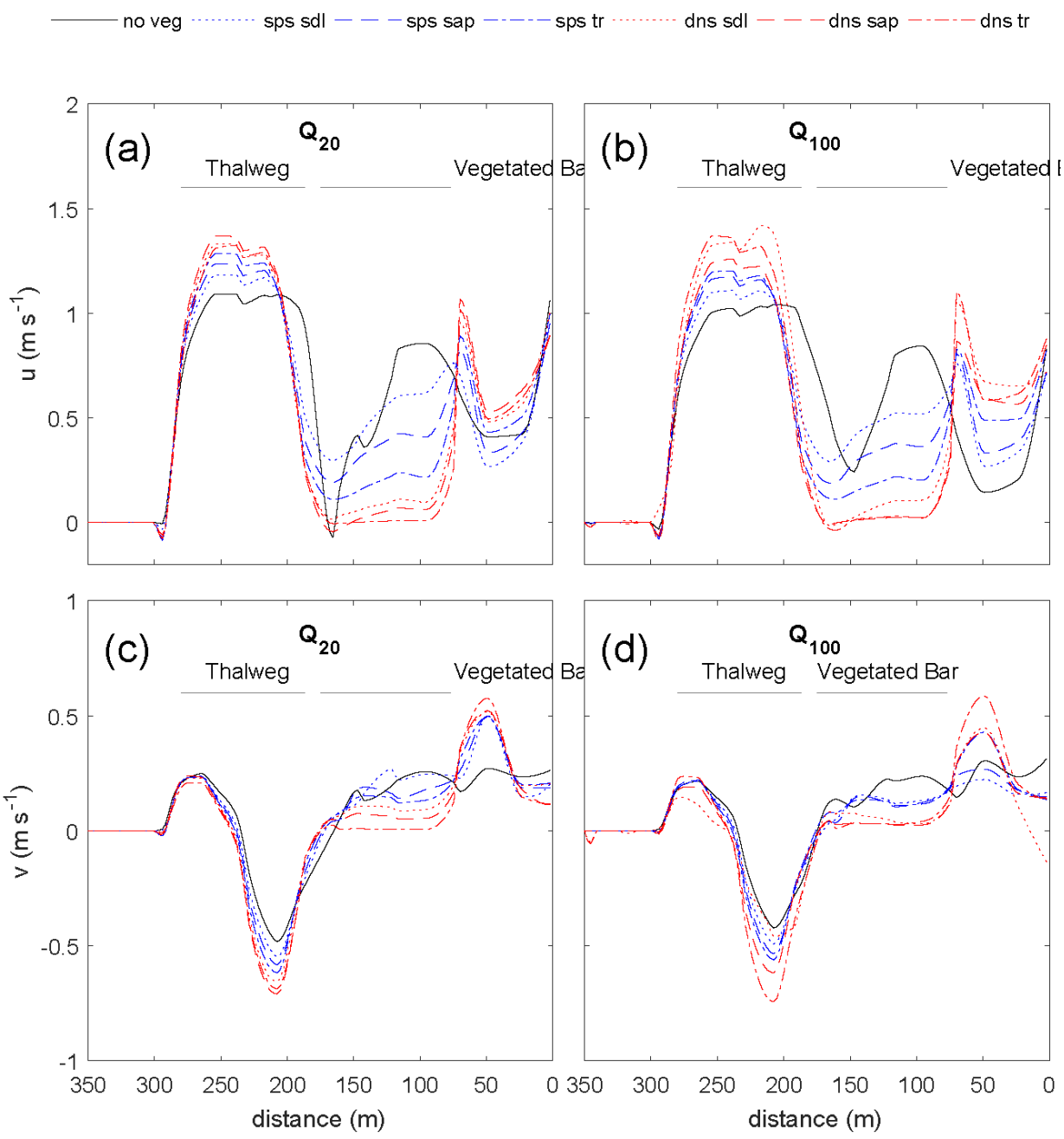

Figure S2. Effect of the vegetated bar (j = 33–75) on the streamwise (u; a,b) and stream-normal (v; c,d) velocity at the downstream cross section (XS1) for the Q_{20} (a,c) and Q_{100} (b,d) flows, with distance from river right end point (Figure 4). With increasing discharge, plant size (seedling to young trees) and density, u is increased and v decreased within the thalweg (j = 100). Both u and v (positive downstream and toward left bank, respectively) are decreased over the bar, and for the sparse young trees and all dense scenarios increased at the edge of the patch. The results for the Q_{20} and Q_{100}, shown here, are similar to the Q_{10} results (Figure 5).

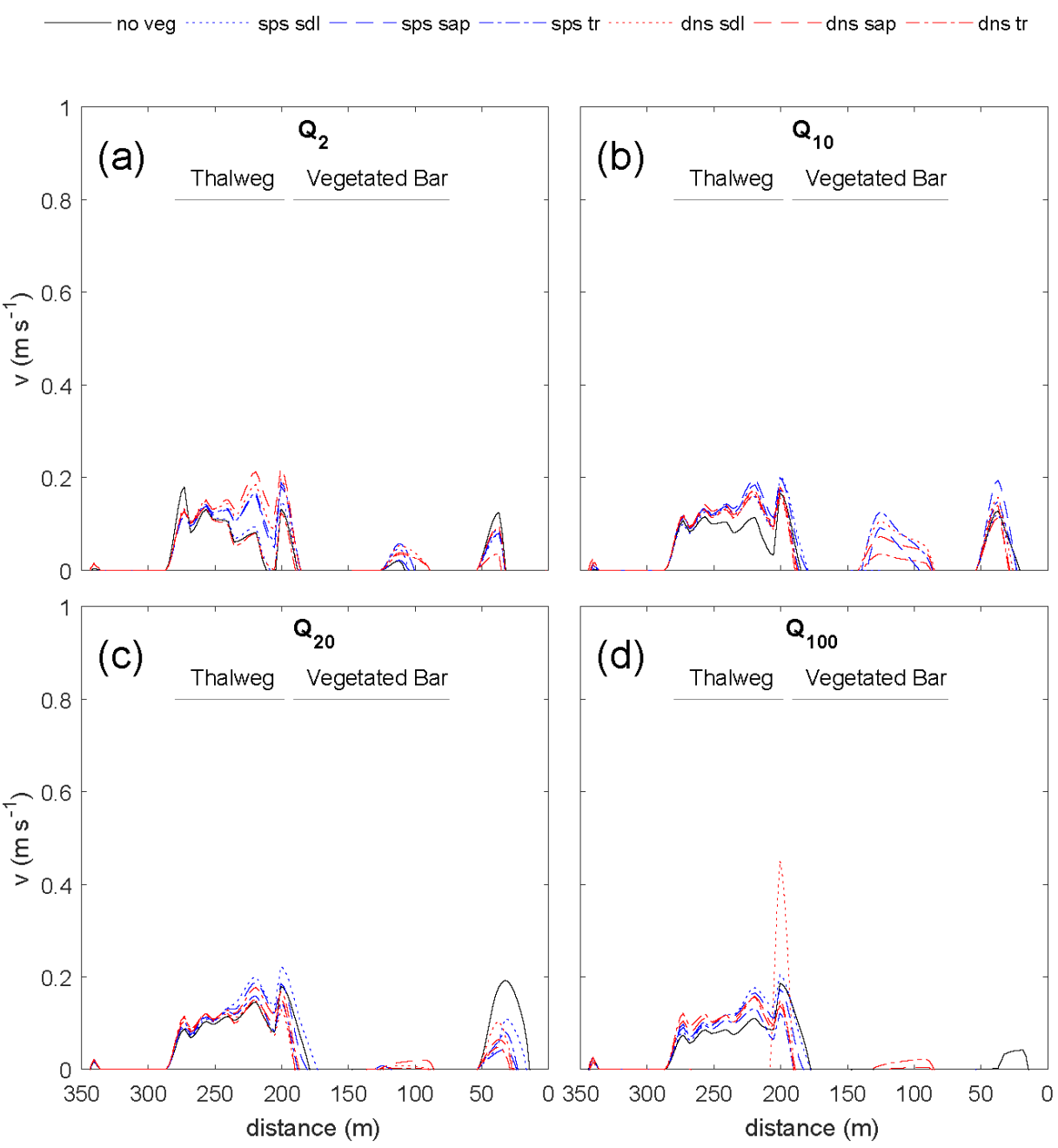
no veg
sps sdl
sps sap
sps tr
dns sdl
dns sap
dns tr
(a)
Q_2
Thalweg
Vegetated Bar
(b)
Q_{10}
Thalweg
Vegetated Bar
(c)
Q_{20}
Thalweg
Vegetated Bar
(d)
Q_{100}
Thalweg
Vegetated Bar
v (m s^{-1})
0
0.2
0.4
0.6
0.8
1
350
300
250
200
150
100
50
0
distance (m)

94

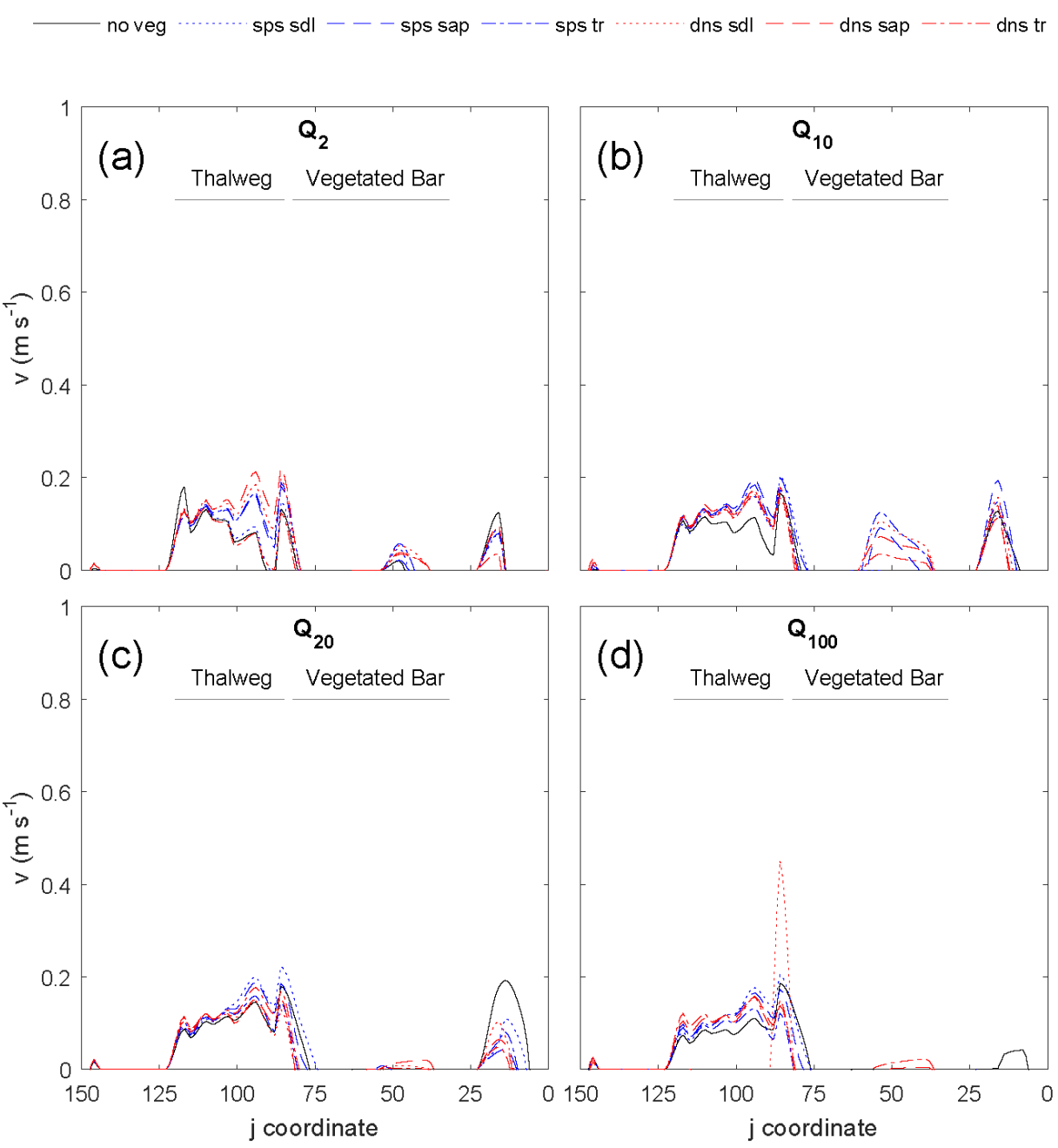

Figure S3. Effect of the vegetated bar (j = 32–82) on the stream-normal (*v*) velocity at the midstream cross section (XS2) for the Q_2 (a), Q_{10} (b), Q_{20} (c), and Q_{100} (d) flows, with distance from river right end point (Figure 4). In general, *v* values are much smaller than *u* values at XS2 (see Figure 6), and not substantially influenced by bar vegetation.

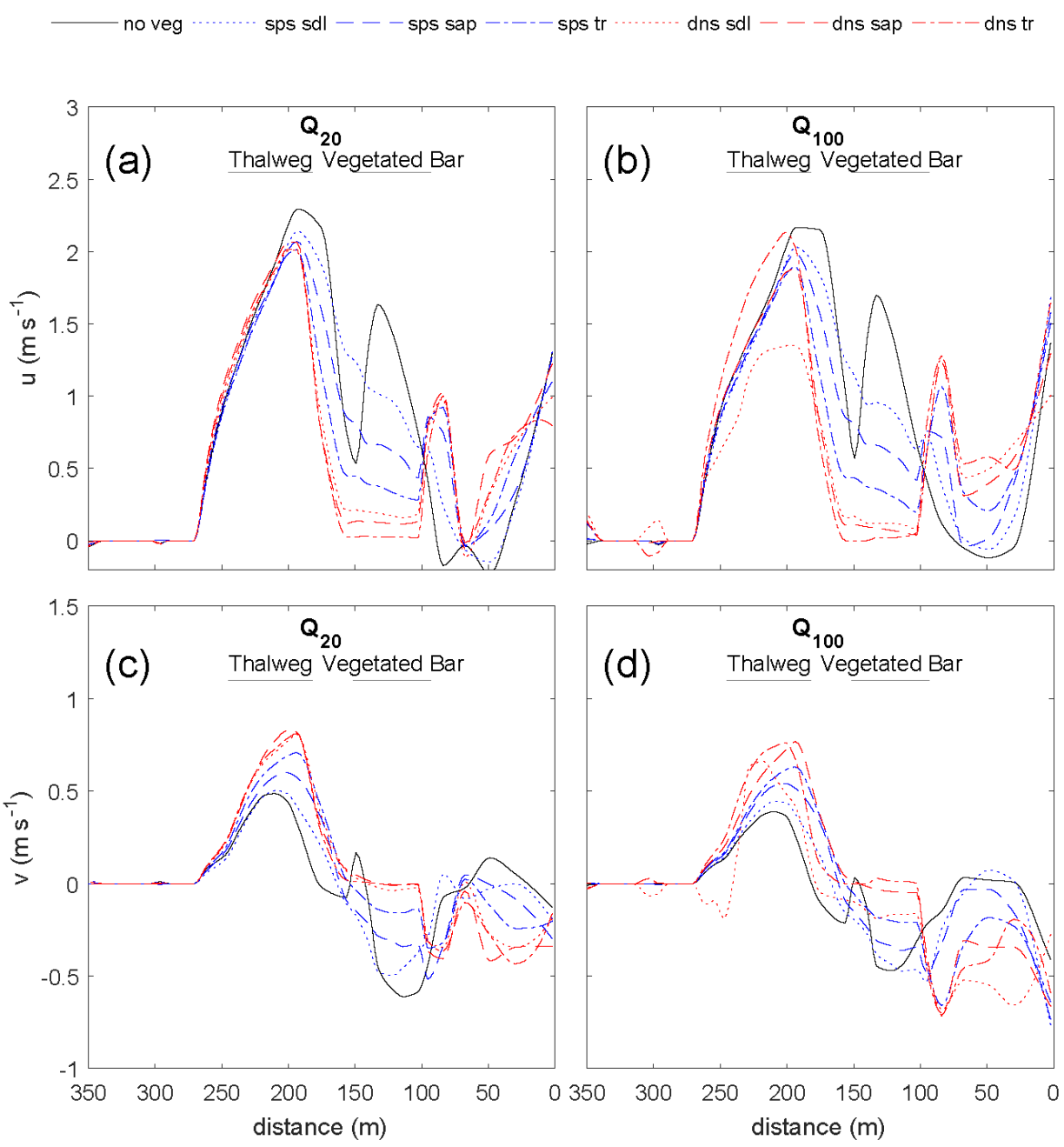
no veg
sps sdl
sps sap
sps tr
dns sdl
dns sap
dns tr
(a)
Q_{20}
Thalweg Vegetated Bar
(b)
Q_{100}
Thalweg Vegetated Bar
(c)
Q_{20}
Thalweg Vegetated Bar
(d)
Q_{100}
Thalweg Vegetated Bar
u (m s^{-1})
v (m s^{-1})
distance (m)
distance (m)

100

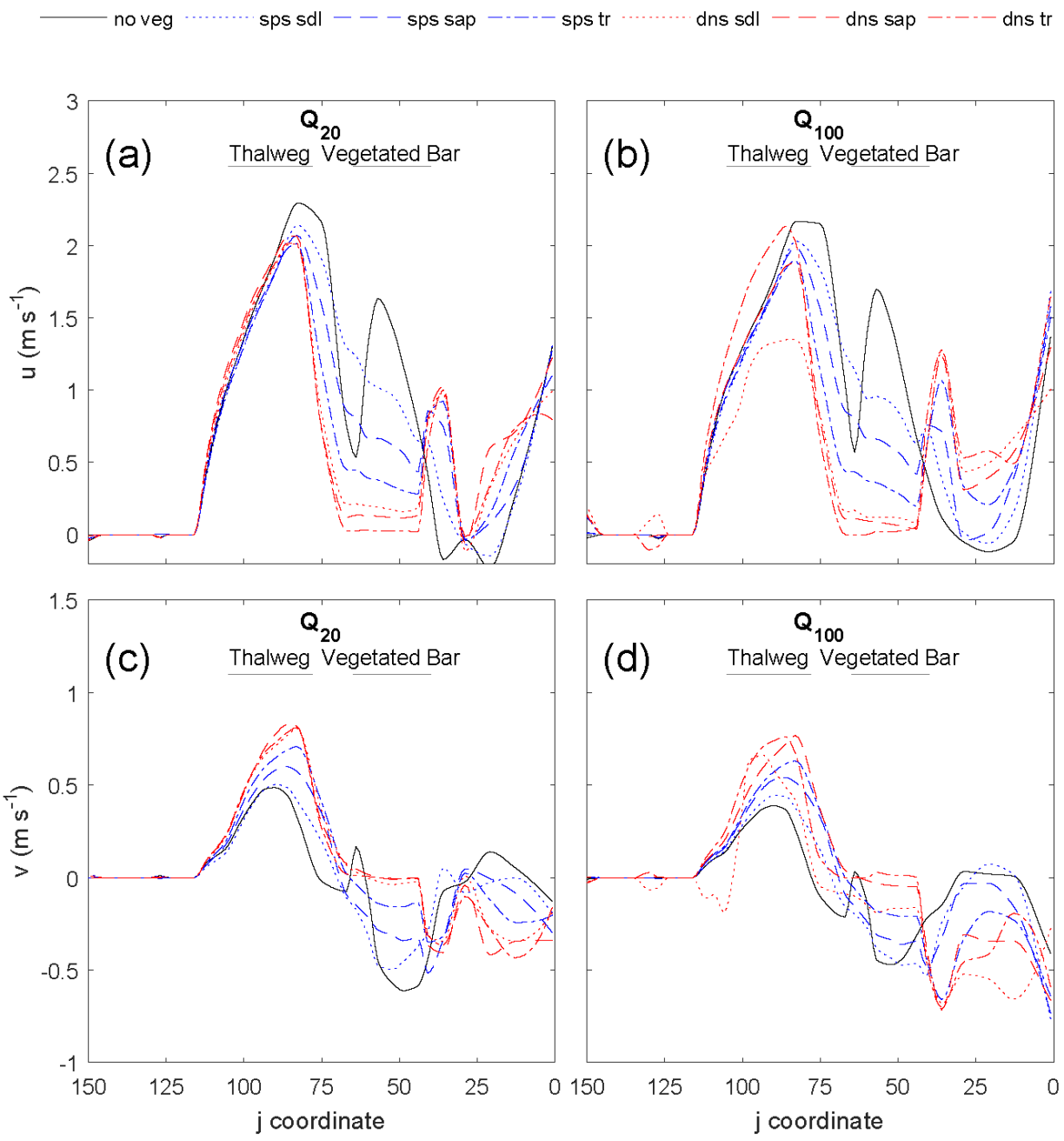

Figure S4. Effect of the vegetated bar (j = 50–65) on the streamwise (*u*; a,b) and stream-normal (*v*; c,d) velocity at the upstream cross section (XS1) for the Q_{20} (a,c) and Q_{100} (b,d) flows, with distance from river right end point (Figure 4). In the thalweg (j = 90) and at the head of the bar, *u* is decreased with increasing seedling size and density. For $Q \geq Q_{10}$, *v* became more negative adjacent to the vegetation patch. The results for the Q_{20} and Q_{100} are similar to that of the Q_{10} flow (shown in Figure 7).

List of terms

A_c = vegetation frontal area (m^2)

c_{Uz} = intercept from regression of U as a function of z

m_{Uz} = slope of regression of U as a function z

u_* = shear velocity

$u_{*_{Uz}}$ = shear velocity calculated from regression U as a function of z

$\bar{U}$ = depth-averaged velocity ($m\ s^{-1}$)

U = velocity ($m\ s^{-1}$)

z_m = height above bed corresponding to law-of-wall-predicted average velocity

z_o = roughness height (m)

$z_{o_{Uz}}$ = roughness height (m) determined from regressing U as a function of z

κ = von Karman constant

References cited

Bergeron, N. and Abrahams, A.: Estimating shear velocity and roughness length from velocit profiles, Water Resour. Res., 28(8), 2155–2158, 1992.

Hemery, G. E., Savill, P. S. and Pryor, S. N.: Applications of the crown diameter–stem diameter relationship for different species of broadleaved trees, For. Ecol. Manage., 215(1–3), 285–294, doi:10.1016/j.foreco.2005.05.016, 2005.

Koch, B., Heyder, U. and Weinacker, H.: Detection of Individual Tree Crowns in Airborne Lidar Data, Photogramm. Eng. Remote Sens., 72(4), 357–363, doi:10.14358/PERS.72.4.357, 2006.

Rennie, C. D. and Church, M.: Mapping spatial distributions and uncertainty of water and sediment flux in a large gravel bed river reach using an acoustic Doppler current profiler, J. Geophys. Res., 115(F3), doi:10.1029/2009JF001556, 2010.

Rennie, C. D. and Millar, R. G.: Measurement of the spatial distribution of fluvial bedload transport velocity in both sand and gravel, Earth Surf. Process. Landforms, 29(10), 1173–1193, doi:10.1002/esp.1074, 2004.

Venditti, J. G., Domarad, N., Church, M. and Rennie, C. D.: The gravel-sand transition: Sediment dynamics in a diffuse extension, J. Geophys. Res. Earth Surf., 120, 1–21,

141 doi:10.1002/2014JF003328.Received, 2015.

142

143